Acta Pharmaceutica Sinica B 2025;15(3):1571−1588

Chinese Pharmaceutical Association
Institute of Materia Medica, Chinese Academy of Medical Sciences

Acta Pharmaceutica Sinica B

www.elsevier.com/locate/apsb
www.sciencedirect.com

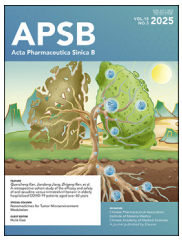

ORIGINAL ARTICLE

eIF3a function in immunity and protection against severe sepsis by regulating B cell quantity and function through m^{6}A modification

Qianying Ouyang[a,b,c,d,e,†], Jiajia Cui[a,b,c,d,f,g,†], Yang Wang[h], Ke Liu[a,b,c,d], Yan Zhan[a,b,c,d], Wei Zhuo[a,b,c,d,i], Juan Chen[h], Honghao Zhou[a,b,c,d], Chenhui Luo[j], Jianming Xia[k], Liansheng Wang[a,b,c,d], Chengxian Guo[l,*], Jianting Zhang[m,*], Zhaoqian Liu[a,b,c,d,*], Jiye Yin[a,b,c,d,*]

[a]*Department of Clinical Pharmacology, Hunan Key Laboratory of Pharmacogenetics, Xiangya Hospital, Central South University, Changsha 410008, China*
[b]*Institute of Clinical Pharmacology, Central South University, Changsha 410078, China*
[c]*Engineering Research Center of Applied Technology of Pharmacogenomics, Ministry of Education, Central South University, Changsha 410078, China*
[d]*National Clinical Research Center for Geriatric Disorders, Xiangya Hospital, Central South University, Changsha 410008, China*
[e]*Department of Lymphoma & Hematology, Hunan Cancer Hospital, the Affiliated Cancer Hospital of Xiangya School of Medicine, Central South University, Changsha 410013, China*
[f]*Department of Geratic Surgery, Xiangya Hospital, Central South University, Changsha 410008, China*
[g]*Department of General Surgery, Xiangya Hospital, Central South University, Changsha 410008, China*
[h]*Department of Pharmacy, Xiangya Hospital, Central South University, Changsha 410008, China*
[i]*Department of Pharmacy, Hunan Traditional Chinese Medical College, Zhuzhou 412000, China*
[j]*Scientific Research Office, Hunan Cancer Hospital, the Affiliated Cancer Hospital of Xiangya School of Medicine, Central South University, Changsha 410013, China*
[k]*Department of Cardiac Surgery, Fuwai Yunnan Hospital, Chinese Academy of Medical Sciences/Affiliated Cardiovascular Hospital of Kunming Medical University, Kunming 650102, China*
[l]*Center of Clinical Pharmacology, the Third Xiangya Hospital, Central South University, Changsha 410017, China*
[m]*Department of Cell and Cancer Biology, University of Toledo College of Medicine and Life Sciences, Toledo, OH 43606, USA*

Received 17 June 2024; received in revised form 6 September 2024; accepted 29 November 2024

*Corresponding authors.
E-mail addresses: yinjiye@csu.edu.cn (Jiye Yin), zqliu@csu.edu.cn (Zhaoqian Liu), jianting.zhang@utoledo.edu (Jianting Zhang), gchxyy@163.com (Chengxian Guo).
[†]These authors made equal contributions to this work.
Peer review under the responsibility of Chinese Pharmaceutical Association and Institute of Materia Medica, Chinese Academy of Medical Sciences.

https://doi.org/10.1016/j.apsb.2025.02.005

KEY WORDS

eIF3a;
m^{6}A;
Sepsis;
B cell;
RNA modification;
Infection;
Translational regulation;
Humoral immunity

Abstract eIF3a is a N^6-methyladenosine (m^{6}A) reader that regulates mRNA translation by recognizing m^{6}A modifications of these mRNAs. It has been suggested that eIF3a may play an important role in regulating translation initiation *via* m^{6}A during infection when canonical cap-dependent initiation is inhibited. However, the death of animal model studies impedes our understanding of the functional significance of eIF3a in immunity and regulation *in vivo*. In this study, we investigated the *in vivo* function of eIF3a using *eIF3a* knockout and knockdown mouse models and found that eIF3a deficiency resulted in splenic tissue structural disruption and multi-organ damage, which contributed to severe sepsis induced by Lipopolysaccharide (LPS). Ectopic eIF3a overexpression in the *eIF3a* knockdown mice rescued mice from LPS-induced severe sepsis. We further showed that eIF3a maintains a functional and healthy immune system by regulating B cell function and quantity through m^{6}A modification of mRNAs. These findings unveil a novel mechanism underlying sepsis, implicating the pivotal role of B cells in this complex disease process regulated by eIF3a. Furthermore, eIF3a may be used to develop a potential strategy for treating sepsis.

1. Introduction

Translation is a complex process of protein synthesis that relies on mRNA information, involving initiation, elongation, termination, and ribosome recycling[1,2]. Of these four steps, initiation is highly regulated and rate-limiting in eukaryotes, primarily controlled by many eukaryotic translation initiation factors (eIFs). Among these eIFs, eIF3 is the most complex factor consisting of 12 subunits (eIF3a to eIF3m) and plays an 'organizing' role in translation initiation. The functions of eIF3 include binding and stabilizing the ternary complex, promoting the binding of the 40S ribosome to mRNAs, and interacting with other eIFs[3]. eIF3a, as the largest subunit of eIF3, participates in translation initiation by directly interacting with elements on mRNAs, including N^6-methyladenosine (m^{6}A) and internal ribosome entry site[4]. eIF3a has also been shown to play numerous important regulatory roles in disease development and therapeutic response[5-8]. For example, eIF3a controls drug sensitivity by regulating the synthesis of DNA repair enzymes[9,10] and the R803K mutation in eIF3a induces cellular senescence and leads to chemotherapy resistance[11].

Recently, it was found that eIF3 is an important m^{6}A reader in mediating cap-independent translation initiation with eIF3a among several subunits that directly bind to m^{6}A[12]. This mechanism bypasses the requirement for a cap and may be important in cases where cap-dependent translation is inhibited, such as during viral infections and in tumorigenesis[12,13]. In another study of L1 retrotransposon mRNA, eIF3a again was found to be one of the three eIF3 subunits that recognizes and binds to m^{6}A modifications and initiates its translation[14]. The mobility of L1 retrotransposon is related to genetic diversity and evolution[15]. Therefore, the cooperation of eIF3a and m^{6}A regulatory systems may be involved in regulating L1 retrotransposons to promote genetic diversity and evolution[14]. In other *in vitro* studies, it has also been shown that eIF3a may interact with other m^{6}A regulators to play a role in diseases, as shown by the combination with METTL16 in regulating occurrence of liver tumors[16]. eIF3a may also initiate translation of circRNAs by recognizing m^{6}A modifications, although this has not been experimentally confirmed[17]. Thus, eIF3a regulates mRNA translation as an m^{6}A reader in a cap-independent manner on mRNAs and circRNAs. With this novel mechanism of regulation, eIF3a may play an important role in disease conditions by regulating protein synthesis.

Despite the advancement in understanding eIF3a function in regulating mRNA translation using biochemical and cell-based studies, such studies using an animal model have not been reported. Here, we used *eIF3a* conditional knockout and knockdown mouse models to investigate its function in physiology and in translational control. Unexpectedly, we found that eIF3a plays a crucial role in the immune system, particularly in the spleen and its deficiency contributed to severe sepsis induced by LPS by regulating B cell production and function *via* m^{6}A modification of mRNAs.

2. Materials and methods

2.1. Materials

Tamoxifen (Sigma−Aldrich) was soluble in anhydrous ethanol and corn oil. The ratio of anhydrous ethanol to corn oil is 1:9, and the final concentration of tamoxifen was 7.5 mg/mL. Lipopolysaccharide (LPS) were purchased from Beyotime and solubilized in phosphate-buffered saline (PBS) with a final concentration of 1 mg/mL. The antibodies (BD Pharmingen) used for flow cytometry CD19 (BD 557398), B220 (BD 553089), CD3e (BD 557596), CD38 (BD 740361), CD138 (BD 558626), CD11B (101241), F4/80(123109), LY-6G (108445) and CD11C (2403221). The antibodies used for immunofluorescence were CD19 (Bioss), the Antifade Mounting Medium with DAPI (Beyotime). The antibodies used for Western blotting are eIF3a (ab86146, Abcam), β-actin (A5441, Sigma), α-tubulin (T9026, Sigma) and GAPDH (G8795, Sigma), HRP-conjugated anti-mouse IgG (AP126P, Sigma) and anti-rabbit IgG (AP510P, Sigma).

2.2. Animal studies

All described animal experiments were permitted by the Experimental Animal Ethics Committee of Xiangya Hospital of Central South University (No: 202311126). Two-month-old SPF C57BL/6J mice were used in this study. All mice were housed in an air-conditioned room with a temperature range of 21−25 °C and subjected to a 12 h light/dark cycle. The mice were divided into different cages based on their age, with each cage containing 8 mice. Water

and food were provided ad libitum to all the mice. Due to the embryonic lethality of *eIF3a* knockout, two conditional knockout models have been created[18]. They are conditional knockout mice *eIF3a*$^{fl/fl}$ *UBC-cre*$^{+}$ mice (abbreviated as *eIF3a*$^{fl/fl}$ mice) and conditional knockdown mice *eIF3a*$^{fl/-}$ *UBC-cre*$^{+}$ mice (abbreviated as *eIF3a*$^{fl/-}$ mice). The strategy involved the deletion of the 2−3 exons of eIF3a using the Cre-loxp system, which was induced by intraperitoneal injection of tamoxifen for five days. *eIF3a*$^{fl/fl}$ *UBC-cre*$^{-}$ or *eIF3a*$^{fl/-}$ *UBC-cre*$^{-}$ mice were used as negative control (NC) mice.

2.3. Datasets

Bulk and single-cell RNA sequencing datasets of sepsis were collected from the Gene Expression Omnibus (GEO) database (https://www.ncbi.nlm.nih.gov/geo/). The bulk RNA sequencing dataset IDs are GSE100159, GSE131761, and GSE134364. The single-cell RNA sequencing (scRNA-seq) dataset ID is GSE175453. Basic information for these datasets is listed in Supporting Information Table S1. Ethical approval was exempted by the institutional ethics committee because all data were obtained from public databases and all patients were de-identified.

2.4. LPS-induced sepsis

Mice were administered intraperitoneally with LPS in PBS at a dosage of 10 mg/kg and monitored for up to 96 h. The low-dose LPS infection was a dosage of 2 mg/kg and monitored for up to 96 h. The clinical score was based on six indicators, including eye discharge, hair erection, diarrhea, tremors, respiratory distress, and drowsiness. Each indication is worth 1 point for a total of 6 points. When the clinical score is greater than 3, it is considered severe sepsis, and $\leq$3 is considered moderate sepsis, a score of 0 indicates no sepsis[19].

2.5. Plaque formation assay

Mice were injected with sheep red blood cells (SRBC), and the spleen was collected four days after injection. The spleen cell suspension was prepared using cell strainers, and then mixed with SRBC and complement. The mixture was injected into a small chamber consisting of two slides sealed with paraffin and incubated at 37 °C for 30 min. The remaining mixture was incubated in a centrifuge tube. SRBC antibodies produced by spleen B cells in the mice triggered hemolysis of the SRBCs. The hemolyzed region in the small chamber exhibits hemolytic plaques, which were observed and counted under a microscope. The tubes were then centrifuged at 1000×*g* for 10 min and the height of the precipitate reflected the amount of undissolved SRBC.

2.6. HE staining

Resected mouse organs were fixed in 4% paraformaldehyde for 24 h and subsequently embedded in paraffin. Sections of 5 μm thickness were cut and mounted on polarized glass slides. These sections were deparaffinized in xylene and rehydrated using a graded ethanol series. Hematoxylin−eosin (HE) Stain Kit (Solarbio) was used for HE staining. Tissue sections were dewaxed twice in a clearing reagent for 5 min each time, then rehydrated with gradient ethanol and finally soaked in distilled water for 2 min. The slice holder was placed in a hematoxylin staining solution for 1 min. Excess stains were washed off with distilled water. The sections were immersed in an eosin staining solution for 1 min and then washed in gradient ethanol.

2.7. Immunofluorescence

The sections were dewaxed twice in the clearing reagent for 5 min each time. Subsequently, the slides were soaked in gradient ethanol, distilled water, and PBS for 2 min each. The citric acid antigen repair solution was prepared in a volume of 400 mL, and the slices were completely submerged in the repair solution. The sections were heated in a microwave oven for 10 min and allowed to cool at room temperature. For IF analysis, tissue sections were permeabilized with PBS for 30 min and then blocked with 10% donkey serum in PBS for 60 min, followed by incubation at 4 °C overnight with primary antibodies diluted in PBS (containing 10% donkey serum). B cell staining was performed using Alexa Fluor 594 labeled CD19 primary antibody. The nuclei were stained with DAPI, and images were captured using the EVOS m7000 Microscope (Thermo Scientific).

2.8. Flow cytometry

The tissue cells were separated using a 70-μm cell strainer, and 2 mL erythrocyte lysate was used to remove erythrocytes. The cells were then re-suspended in PBS and diluted to a concentration of 1×10^7 cells/mL. Finally, 2 μL of antibody was added to 100 μL cell suspension and incubated for 20 min at 4 °C in the absence of light. Detection of samples was performed using the NL3000 machine (Cytek) and analyzed with FlowJo version 10 software (BD). Lymphocyte populations were identified based on their forward scatter (FSC) and side scatter (SSC) characteristics. The markers of cell types include $CD19^+$ $B220^+$ for B Cell, $CD3E^+$ for T cell, $NK1.1^+$ $CD3E^-$ for NK cell, $CD138^+$ $CD38^+$ for plasma cells, $CD1C^+$ $F4/80^-$ for dendritic cell, $CD1B^+$ $F4/80^+$ for macrophage, and $CD1B^+$ $LY\text{-}6G^+$ for neutrophil.

2.9. Quantification of serum cytokines

Mouse tissues were subjected to protein extraction using RIPA, and their concentrations were determined by means of the BCA kit. The proteins were stored at −80 °C prior to conducting ELISA assays for measuring inflammatory cytokines (IL-1, IL-6, IFN-γ) with a Mouse ELISA Kit (Abclonal). The concentration of cytokines was determined using ELISA kits in accordance with manufacturer's instructions. Diluted samples from the blank, control, and *eIF3a*$^{fl/fl}$ mice were added to a 96-well plate. The samples were incubated at 37 °C for 30 min and subsequently washed five times. Enzyme-conjugate reagent was added to each well, except the blank well, followed by the color developing reagent to induce sample coloring. A termination solution was used to halt the reaction when all wells changed from blue to yellow. Finally, OD_{450nm} was determined using a microplate reader (Agilent).

2.10. Western blot

Mouse tissues were lysed using RIPA buffer, and the protein concentration was determined with a BCA kit. Subsequently, the samples were separated on 10% SDS-PAGE gels and transferred onto nitrocellulose membranes (Millipore). The membranes were incubated with antibodies against eIF3a, β-actin, α-tubulin and GAPDH at 4 °C overnight, followed by washing three times with

TBST, and incubation with HRP-conjugated anti-mouse IgG or anti-rabbit IgG at room temperature for 1 h. The signals were developed using electrochemiluminescence reagents (Thermo Scientific) and images were captured using ChemiDoc Imagers (Bio-rad).

2.11. Mass spectrometry

Sera samples from mice were subjected to mass spectrometry experiments. The proteins were desalted using C18 StageTip and subsequently dried before being redissolved with 0.1% formic acid. The protein concentration was determined by measuring OD_{280nm}, followed by trypsin digestion and chromatographic separation of the peptides using the Easy nLC 1200 chromatography system (Thermo Scientific). The buffer solution was made by mixing liquid A (0.1% formic acid in water) with liquid B (80% acetonitrile and water mixture containing 0.1% formic acid). After injection into the Trap Column, sample separation was achieved using the chromatographic column. The flow rate was measured at 300 nL/min, and subsequent peptide analysis was performed using a Q-Exactive HF-X mass spectrometer (Thermo Scientific) with data-dependent acquisition mass spectrometry. Peptides were mapped to proteins and relative peptide scores were calculated using MaxQuant 1.6.17.0 software.

2.12. Quantification of m^6A modifications

The EpiQuik™ m^6A RNA Methylation Quantification Kit (Colorimetric) was used to quantify the m^6A modification. The first step involves lysing the cells or tissues to release the RNA molecules. Then RNA is fragmented into smaller pieces. In m^6A IP step, an m^6A-specific antibody is used to selectively bind to the RNA molecules containing m^6A modifications. The enriched m^6A-modified RNA is eluted and subjected to a colorimetric assay. At last, the colorimetric signal generated in the previous step is measured using a spectrophotometer. The optical density reading indicates the relative abundance of m^6A modifications in the RNA sample.

2.13. MeRIP-seq

Polyadenylated RNA was extracted using RNAiso Plus reagent (Takara). RNA fragment containing m^6A and input RNA fragment was extracted using EpiQuik CUT&RUN m^6A RNA Enrichment Kit (EpigenTek). The amount of total RNA for IP sample was 20 μg. RNA sample, immuno-capture buffer (ICB), m^6A antibody, and affinity beads were mixed and incubated at room temperature for 90 min. Then nuclear digestion enhancer (NDE) and cleavage enzyme mix (CEM) were added and incubated at room temperature for 4 min. After the beads were adsorbed with the magnetic device, the supernatant was discarded. Next, magnetic beads, Proteinase K, and PDB (Protein Digestion Buffer) were mixed and incubated at 55 °C for 15 min to enrich RNA, and the solution was collected on the magnetic device. After that, IP samples were incubated with RNA purification solution, 100% Ethanol, and RNA binding beads at room temperature for 5 min. Then, the IP RNA samples were eluted with the elution buffer after washing with 90% ethanol. The input amount was 10 μg RNA. ICB, CEM, and NDE were mixed and incubated for 2 min at room temperature. Then, RPS, 100% Ethanol and RNA binding beads were added to input tube. Finally, the input RNA samples were eluted with the elution buffer after washing with 90% ethanol. Pair-end sequencing of samples was carried out on the Illumina platform (Illumina).

2.14. MeRIP-qPCR

$eIF3a^{fl/-}$ and control mice were treated with LPS for 12 h after which spleens were taken to make single cell suspensions as described above. Flow cytometry sorting of B cells was performed using CD19 and B220 as markers. 1×10^7 B cells were harvested from each sample, and RNA was extracted by trizol method, followed by MeRIP experiments according to the above steps. For MeRIP RNA and Input RNA, cDNA was obtained by reverse transcription. Expression of m^6A modified fragment was detected by SYBR-green-based qPCR. Primers: YTHDF2 (F-GCCTGGAGCTTTATTGAGGGT, R-TGACTTCTCAGCATG GGGAAAT), YTHDF3 (F-TGGGCTGCTATTGCCAGAAA, R-GAGCCTTTACCAC TGACCCC).

2.15. Bioinformatics analysis

2.15.1. scRNA sequencing analysis

All analyses were done using R version 4.1.2 and Seurat version 4.1.0. A Seurat object was created with default parameters. Only cells expressing 200−6000 genes with each gene expressed in >10 cells, $\log_{10}$Genes Per UMI >0.80, and mitochondrial genes <10% were used, resulting in a final object containing 29,247 cells. The data was normalized by the expression, multiplied by a scale factor of 10,000 and log-transformed. The 2000 most variable genes based on standardized variance were selected for principal component analysis (PCA) as an initial dimensional reduction. To account for biological batch differences between the scRNA-seq libraries, the Seurat anchor-based integration method for merging datasets was utilized. The integration anchors were then identified from the first 20 dimensions and then used to generate a new dimensional reduction. The scaled integrated data matrix was further reduced to two-dimensional space using PCA followed by t-distributed stochastic neighbor embedding (tSNE) for visualization. Clusters were assigned known broad cell types based on the expression of defined population markers. The markers used to annotate cell types include CD3E for T cell, CD19 and CD79A for B, CD1C for dendritic cell, MZB1 for plasma cells, and CD14 and CD68 for monocytes.

2.15.2. MeRIP-seq sequencing analysis

Raw data of fastq format were processed using fastp software. Clean data were obtained by removing reads containing adapter, ploy-N, and low-quality reads from raw data. Reference genome (GRCm39) and gene model annotation files were downloaded from the genome website. MACS2 version 2.1.0 was utilized for peak calling, which identified regions of MeRIP enrichment over background. Fold enrichment was used to indicate the m^6A modification in the IP sample compared with the input sample. Homer and MEME were used to detect the motifs. m^6A-modified fragments were annotated by PeakAnnotator and RNAmod[20,21]. The analysis of differential peaks was performed using the exomePeak2 software[22].

2.15.3. RNA-seq sequencing analysis

Input RNA of MeRIP was used for RNA-seq analysis. STAR aligner was used to map sequencing reads to transcripts in the mouse reference genome GRCm39. Read counts for individual transcripts were produced by RSEM. EdgeR was used to estimate

expression values and detect differentially expressed transcripts. Transcript expression levels were dichotomized by the median level with $\log_2$Fold change >1 and *P*-value <0.05 considered statistically significant. Cell states were predicted by EcoTyper[23]. Metascape website was used for functional enrichment[24].

2.16. Statistical analysis

All experimental data were obtained from at least three independent biological repeats and presented as mean ± standard deviation (SD). Statistical graphs were drawn using the software GraphPad Prism 8.01 (GraphPad Software) Data statistics were performed using SPSS statistic 22 (IBM). Log-rank test was performed to assess the association between transcript expression of eIF3a and disease state. Statistical comparisons between two groups were accessed by a two-tailed student's *t*-test or two-sided Mann−Whitney test. The Spearman and Pearson correlation tests were used to assess relationships between variables in tumor tissues. Statistical significance was defined as *P* values of <0.05.

3. Results

3.1. eIF3a deficiency triggers systemic inflammatory response

Because eIF3a deficiency leads to mouse embryonic lethality[18], we generated *eIF3a* conditional knockout mice using *eIF3a*$^{fl/fl}$ *UBC-Cre* (hereafter referred to as *eIF3a*$^{fl/fl}$) induced by tamoxifen (Fig. 1A)[18]. Supporting Information Fig. S1A shows that eIF3a is ubiquitously expressed in all major organs of the wild-type mice as determined using Western blot. After 5 days of tamoxifen treatment, eIF3a expression is dramatically reduced in all tested organs of the *eIF3a*$^{fl/fl}$ mice (Fig. S1B), suggesting that induced deletion of eIF3a gene is successful. However, eIF3a was not depleted in some organs due to insufficient time as all mice died on Day 8 after tamoxifen induction (see below).

The *eIF3a*$^{fl/fl}$ mice suffered severe body weight loss beginning on Day 4 after tamoxifen administration (Fig. 1B) and began to die on Day 6 and all died on Day 8 (Fig. 1C). However, the body weight of the negative control mice was not affected by tamoxifen injection (Fig. 1B) and none of them died during this period of treatment (Fig. 1C). Therefore, all mice were harvested on Day 6 for analysis. Interestingly, all *eIF3a*$^{fl/fl}$ mice showed significant hypothermia on Day 6 before sacrifice, with an average rectal temperature below 34 °C (Fig. 1D), compared with ∼37 °C for the control mice. On Days 4 and 5, the *eIF3a*$^{fl/fl}$ mice gradually became inactive, and on Day 6 they significantly curled up before death (Fig. 1E). In addition, the eyes of the *eIF3a*$^{fl/fl}$ mice appeared to be closed with secretions, and the hairs on the head and back were disheveled and erected with apparent evidence of diarrhea in the anus area (Fig. 1F).

Next, gross anatomy and pathological analyses of internal organs were performed. Fig. 1G shows that the spleen and thymus of *eIF3a*$^{fl/fl}$ mice were much smaller than those of control mice, with diameters of 10 and 4 mm, respectively, compared with 14 and 7 mm in control mice. Moreover, the *eIF3a*$^{fl/fl}$ mice presented swollen guts and thinned gut walls. Most of the internal organs showed a decrease in relative weight with spleen and thymus dropping the most by >50% (Fig. 1H). The *eIF3a*$^{fl/fl}$ mice also had a significant decrease in the number of lymphocytes, but not of neutrophils and monocytes (Fig. 1I) as determined using complete blood count (CBC). This finding was confirmed using flow cytometry, which showed that the proportion of lymphocyte populations in the *eIF3a*$^{fl/fl}$ mice was significantly lower than that in the control mice. The average lymphocyte count in the *eIF3a*$^{fl/fl}$ mice accounted for only 5% of the total viable cells in whole blood compared to 23% in the control mice (Fig. 1J). It is known that lymphocytes mainly consist of B cells and T cells. We further analyzed the proportions of B cells and T cells within the lymphocyte population using flow cytometry. The results revealed that the percentage of B cells in the peripheral blood of *eIF3a*$^{fl/fl}$ mice (23%) was significantly lower compared to the control mice (47%) (Fig. S1C).

Since the spleen and thymus were affected the most, we next performed HE-staining analysis of these two organs. As shown in Fig. 1K, the boundaries between the cortical and medullary regions in the thymus of the *eIF3a*$^{fl/fl}$ mice disappeared, causing relocation of cortical cells to the central medulla region. The size and density of the white pulp in the spleen of the *eIF3a*$^{fl/fl}$ mice were reduced and the boundary between the white and red pulp was indistinct. The average area of white pulp in the spleen of the *eIF3a*$^{fl/fl}$ mice was 0.3×10^3 μm^2, which is significantly lower than that in the control mice with 1.5×10^3 μm^2. Other organs of the *eIF3a*$^{fl/fl}$ mice also exhibited varying degrees of damage (Fig. 1L). Alveolar atrophy and inflammatory cell infiltration were found in the lungs. Hepatic lobular structure disorder and hepatocellular edema were found in the livers. The renal tubular epithelial cells in the kidneys were swollen, and there was inflammatory cell infiltration in the glomeruli with congested capillaries. In the intestines, the number of cup cells decreased and intestinal microvilli disappeared. Epithelial necrosis was found in the colon, and sperm dysplasia was found in the testis. No significant abnormalities were observed in the cardiac or skeletal muscles (Fig. S1D). Blood biochemical analysis revealed elevated levels of ALT and AST in *eIF3a*$^{fl/fl}$ mice, indicating liver injury. Elevated levels of CKMB indicated cardiac damage, while increased levels of CRP suggested acute infection or tissue damage. No abnormalities were observed in kidney function (Fig. S1E).

Furthermore, the blood levels of three classical inflammatory factors (IL-1, IL-6, and IFN-γ) were detected to investigate the inflammatory response. Fig. 1M shows that the concentration of all three factors in the blood is significantly elevated in the *eIF3a*$^{fl/fl}$ mice. Together, we conclude that eIF3a deficiency may result in immune system abnormalities and multi-organ damage.

3.2. Impact of eIF3a knockdown on inflammatory response

As homozygous knockout mice exhibited immune system abnormalities and multi-organ damage and died within a short period of induced eIF3a deletion, we resorted to heterozygous mice (referred to as *eIF3a*$^{fl/-}$) to investigate the impact of *eIF3a* knockdown. For this experiment, the *eIF3a*$^{fl/-}$ mice were treated with tamoxifen for 5 days, followed by analysis or sacrifice on Day 15 (Supporting Information Fig. S2A and S2B). Firstly, similar to the *eIF3a*$^{fl/fl}$ mice, the *eIF3a*$^{fl/-}$ mice had curled posture with disheveled hair (Fig. S2C) due to systematic *eIF3a* knockdown in all organs examined. Interestingly, these mice had no obvious abnormalities in their eyes or anus (Fig. S2C) or change in survival (Fig. S2D), body weight (Fig. S2E), and rectal temperature compared with the control mice (Fig. S2F). Analyses of the gross anatomy revealed that most organs in the *eIF3a*$^{fl/-}$ mice were similar to those of control mice except the spleen, which was shorter in the *eIF3a*$^{fl/-}$ mice than that of the control mice (Fig. S2G). This observation is consistent with the relative weight

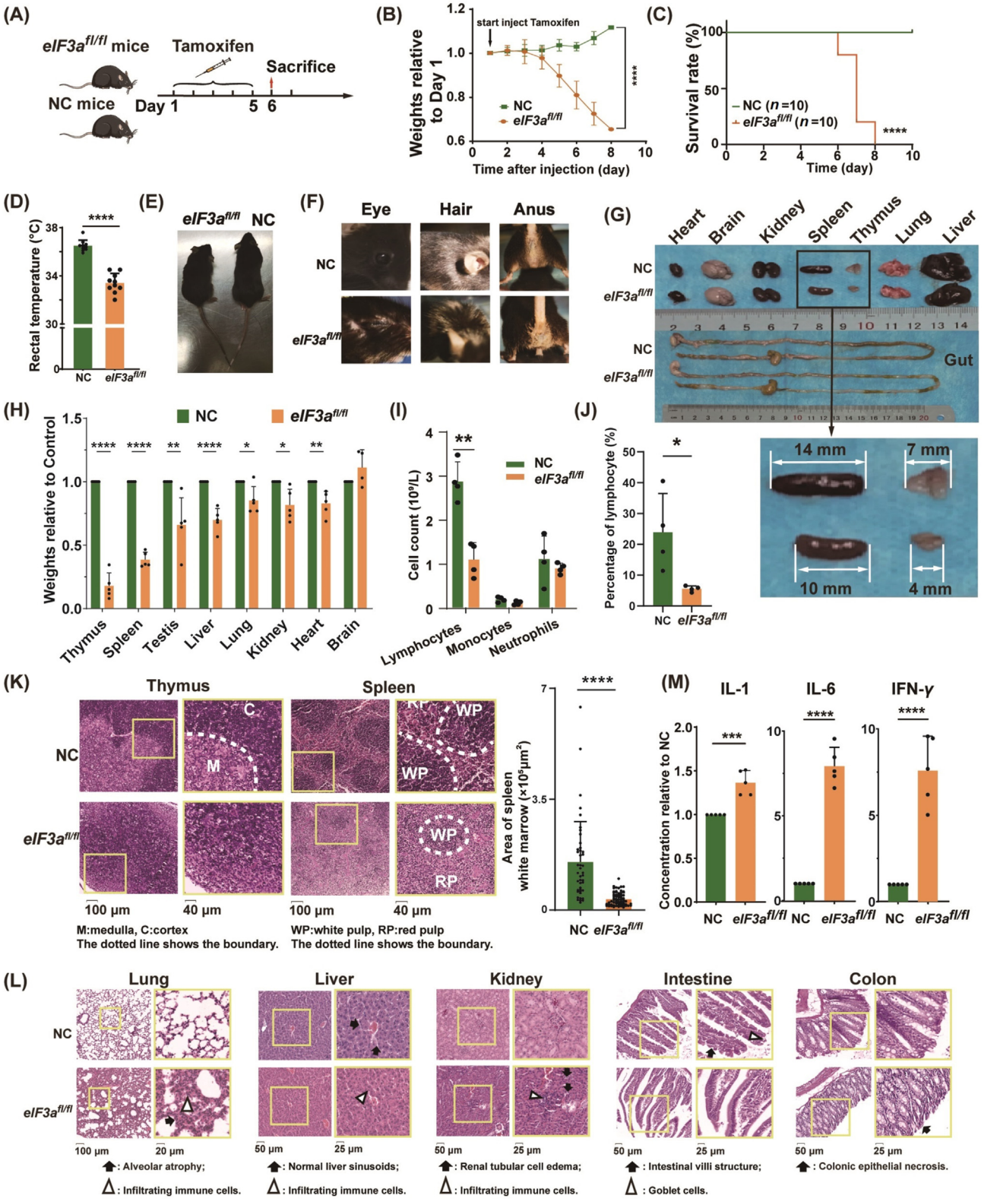

Figure 1 *eIF3a* knockout and severe multi-organ inflammatory responses. (A) Scheme of *eIF3a* knockout induction *via* intraperitoneal injection of tamoxifen. (B−F) Body weight change (B), overall survival (C) of $eIF3a^{fl/fl}$ and control (NC) mice, and rectal temperatures (D), body posture (E), status of eye, hair, and anus (F) on Day 6. (G, H) Gross anatomy (G) and relative weight (H) of major organs from $eIF3a^{fl/fl}$ and control (NC) mice. (I, J) Number of monocytes, neutrophils, and lymphocytes as determined by counting (I) and relative lymphocytes determined by flow cytometry (J) using blood from $eIF3a^{fl/fl}$ and control (NC) mice on Day 6. (K, L) Images of HE-stained thymus and spleen (K) and other organ (L) sections. White pulp areas in the spleen were quantified and shown in panel (K). (M) The relative concentration of IL-1, IL-6, IFN-γ in serum of $eIF3a^{fl/fl}$ and control (NC) mice on Day 6. Data are presented as means ± SD ($n = 5$); $^{*}P < 0.05$, $^{**}P < 0.01$, $^{***}P < 0.001$, $^{****}P < 0.0001$.

of each organ in these mice (Fig. S2H). Furthermore, CBC results implied that *eIF3a*$^{fl/-}$ mice had a higher lymphocyte count than control mice (Fig. S2I). Due to significant differences in spleen size, we isolated the spleens into single cells and analyzed the proportions of multiple cells (B cells, T cells, NK cells, macrophages, neutrophils and DC cells) by flow cytometry, which showed that only the proportion of B cells was less than that of controls in the *eIF3a*$^{fl/-}$ mice, and there were no significant differences in the proportions of any other cells (Fig. S2J and S2K).

The major organs were also stained with HE for pathological analysis. As shown in Supporting Information Fig. S3A, the thymus of the *eIF3a*$^{fl/-}$ mice showed no abnormality, different from that of the *eIF3a*$^{fl/fl}$ mice. However, compared with the control mice, the spleen of the *eIF3a*$^{fl/-}$ mice showed a reduction in cell density and white pulp area with two-thirds remaining, and a blurred junction with red pulp, which are similar to the observations of the spleen in *eIF3a*$^{fl/fl}$ mice. Pathological changes with inflammation were also evident in other organs of the *eIF3a*$^{fl/-}$ mice, including alveolar atrophy and pulmonary interstitial lymphocyte infiltration, loss of liver sinuses and inflammatory cell infiltration around the central hepatic vein, and loss of intestinal microvilli (Fig. S3B). There is no remarkable change in the kidney, colon, testis, and muscle. Finally, IFN-γ in the blood of *eIF3a*$^{fl/-}$ mice was approximately 1.5 times higher than that in the control mice although that of IL-1 and IL-6 did not change (Fig. S3C). The blood biochemical results showed an elevation in CREA levels in *eIF3a*$^{fl/-}$ mice, suggesting possible kidney damage.

In summary, the *eIF3a*$^{fl/-}$ mice showed a mild abnormality, characterized by splenic white pulp shrinkage, multi-organ damage, and increased blood inflammatory factors, but to a lesser extent overall than that in the *eIF3a*$^{fl/fl}$ mice. Thus, reduced eIF3a levels likely lead to immune system abnormalities and multi-organ damage, the severity positively associated with the degree of eIF3a reduction.

3.3. *eIF3a function in protection against sepsis*

As both the *eIF3a*$^{fl/fl}$ and *eIF3a*$^{fl/-}$ mice exhibited different degrees of immune system abnormalities, we hypothesize eIF3a may play a role in inflammatory response. Therefore, we used sepsis, a classical model of infection-induced systemic inflammatory disease, to investigate the impact of *eIF3a* knockdown on the induced inflammatory response in the *eIF3a*$^{fl/-}$ mice. We first tested sepsis induction using intraperitoneal injection of LPS in the negative control and *eIF3a*$^{fl/-}$ mice without induction of *eIF3a* knockdown. As shown in Supporting Information Fig. S4, inflammatory responses were observed on the body surface of mice 24 h after LPS injection. Both the negative control and *eIF3a*$^{fl/-}$ mice also developed sepsis after LPS injection compared with control PBS-treated mice as determined by evaluating clinical scores of sepsis severity. Thus, LPS could successfully induce sepsis in these mice.

Next, the LPS-induced sepsis was used to compare the negative control and *eIF3a*$^{fl/-}$ mice following induction of *eIF3a* knockdown. Ten days after tamoxifen injection to induce *eIF3a* knockdown, both groups of mice were treated with one bolus dose of LPS followed by various analyses (Fig. 2A). As shown in Fig. 2B, typical septic phenotypes were observed in both *eIF3a*$^{fl/-}$ and control mice. However, *eIF3a*$^{fl/-}$ mice exhibited more severe eye discharge and the hairs on their backs were sparse and erect, exposing their skins whereas the control mice had slightly erect hair on their neck. Additionally, the *eIF3a*$^{fl/-}$ mice exhibited more severe diarrhea (Fig. 2B). The severity of sepsis was also assessed using a clinical score system (see Method). As shown in Fig. 2C, the control mice had an average score of 3, indicating moderate sepsis, while the *eIF3a*$^{fl/-}$ mice had an average score of 5, indicating severe sepsis at 24 h after LPS injection. For the first 36 h after LPS injection, both groups experienced similar weight loss (Fig. 2D). However, the body weight recovery after 36 h is slower for *eIF3a*$^{fl/-}$ mice than the control animals (Fig. 2D). Both the control and *eIF3a*$^{fl/-}$ mice also exhibited hypothermia at 12 h after LPS injection (Fig. 2E). However, the rectal temperature of *eIF3a*$^{fl/-}$ mice remained consistently lower than that of the control mice thereafter. Furthermore, the *eIF3a*$^{fl/-}$ mice had a higher mortality rate with more than 50% of mice dead at 72 h after LPS injection compared with 20% in the control group (Fig. 2F).

The spleen of the *eIF3a*$^{fl/-}$ mice appears slightly smaller and lighter in color than those of the control mice, indicating a reduction in splenic parenchyma. Other major organs (heart, brain, kidney, lung, liver, and intestine) of the *eIF3a*$^{fl/-}$ mice exhibited more swelling compared to those of the control group (Fig. 2G). Furthermore, the *eIF3a*$^{fl/-}$ mice had a more severe pulmonary hemorrhage. The number of lymphocytes in the *eIF3a*$^{fl/-}$ mice was about half of that in the control mice, while the numbers of monocytes and neutrophils were similar to those in the control group (Fig. 2H).

Pathological analysis of tissue sections showed inflammatory damage in various organs. The white pulp area in the spleen of the *eIF3a*$^{fl/-}$ mice shrunk to about one-third of that in the control mice (Fig. 2I). Furthermore, the white pulp of the *eIF3a*$^{fl/-}$ mice exhibited more debris from nuclei and cytoplasm, fewer intact cells, and more red blood cells compared to the control mice. The ratio of the necrotic region to white pulp area in the *eIF3a*$^{fl/-}$ mice was significantly higher than that in the control mice (Fig. 2I). These results suggest that the *eIF3a*$^{fl/-}$ mice likely experienced more severe sepsis that led to spleen necrosis. Additionally, the lungs, livers, hearts, intestines, and colons also appeared to have more severe inflammation in the *eIF3a*$^{fl/-}$ mice (Fig. 2J). The lungs of the *eIF3a*$^{fl/-}$ mice exhibited more alveolar exudation, alveolar atrophy, and infiltration of inflammatory cells. In the livers of the *eIF3a*$^{fl/-}$ mice, hepatic sinuses disappeared and there was infiltration of inflammatory cells. Increased capillary congestion and infiltration of inflammatory cells in the interstitial myocardial cells, decreased intestinal cup cells and increased colonic epithelial necrosis were also observed in the *eIF3a*$^{fl/-}$ mice. Renal cell edema and glomerular inflammatory cell infiltration did not differ significantly between the two groups. It was also found that the levels of inflammatory factors including IL-1, IL-6, and IFN-γ were all higher in the serum (Fig. 2K) and organs (Supporting Information Fig. S5A) of the *eIF3a*$^{fl/-}$ mice than in the control animals. Finally, we induced low-dose LPS infection in *eIF3a*$^{fl/-}$ mice and control mice, with fever being the main characteristic. Similarly, *eIF3a*$^{fl/-}$ mice exhibited more pronounced body temperature elevation and weight loss, indicating a more severe inflammatory response (Fig. S5B and S5C).

Combined with these results, mice with reduced eIF3a developed more severe sepsis and had a higher mortality rate than control mice after LPS induction. eIF3a expression may play a crucial role in mouse resistance to sepsis.

3.4. *eIF3a inhibits sepsis through m^{6}A regulation*

As eIF3a is an important m^{6}A reader, we investigated the regulatory mechanism of eIF3a in immunity by identifying its target

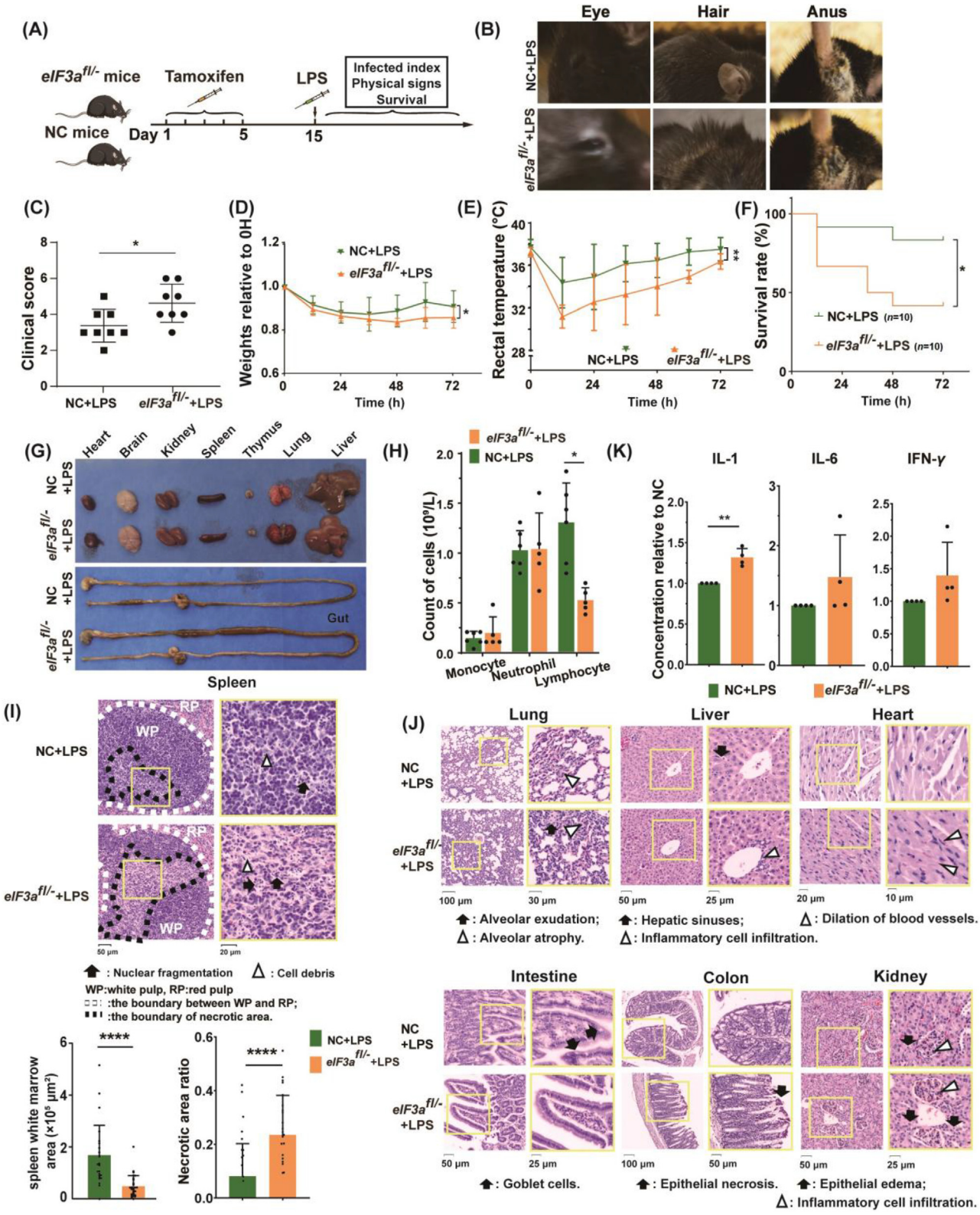

Figure 2 Development of severe LPS-induced sepsis in the *eIF3a*$^{fl/-}$ mice. (A) Scheme of sepsis induction by LPS in the *eIF3a*$^{fl/-}$ and control mice. (B–F) Status of eye, hair, and anus (B), clinical scores of sepsis 24 h after LPS injection (C), body weight change (D), rectal temperatures (E), and overall survival (F) of the *eIF3a*$^{fl/-}$ and control (NC) mice following LPS injection. (G) Gross anatomy of major organs in the *eIF3a*$^{fl/-}$ and control mice after sepsis induction. (H) Monocyte, neutrophil, and lymphocyte counts in mouse PBMC 24 h after LPS injection. (I, J) Images of HE-stained sections of the spleen (I) and other organs (J) of the control and *eIF3a*$^{fl/-}$ mice. Quantifications of white pulp and necrotic areas in the spleen of the two groups are shown in panel (I). (K) Relative concentrations of IL-1, IL-6, and IFN-γ in the serum of both groups at 24 h after LPS injection. Data are presented as means ± SD ($n = 5$); $^{*}P < 0.05$, $^{**}P < 0.01$, $^{****}P < 0.0001$.

genes with m^{6}A modifications. For this purpose, we first used a colorimetric assay to quantify m^{6}A levels in the spleen of our mice and found that the total m^{6}A modification was significantly lower in the *eIF3a*$^{fl/fl}$ mice compared to the control mice (Fig. 3A). This finding suggests that eIF3a may regulate m^{6}A modification directly or indirectly. Subsequently, we devised a methylated RNA immunoprecipitation sequencing (MeRIP-seq) to investigate the regulation of m^{6}A by eIF3a in sepsis. Consequently, the *eIF3a*$^{fl/-}$

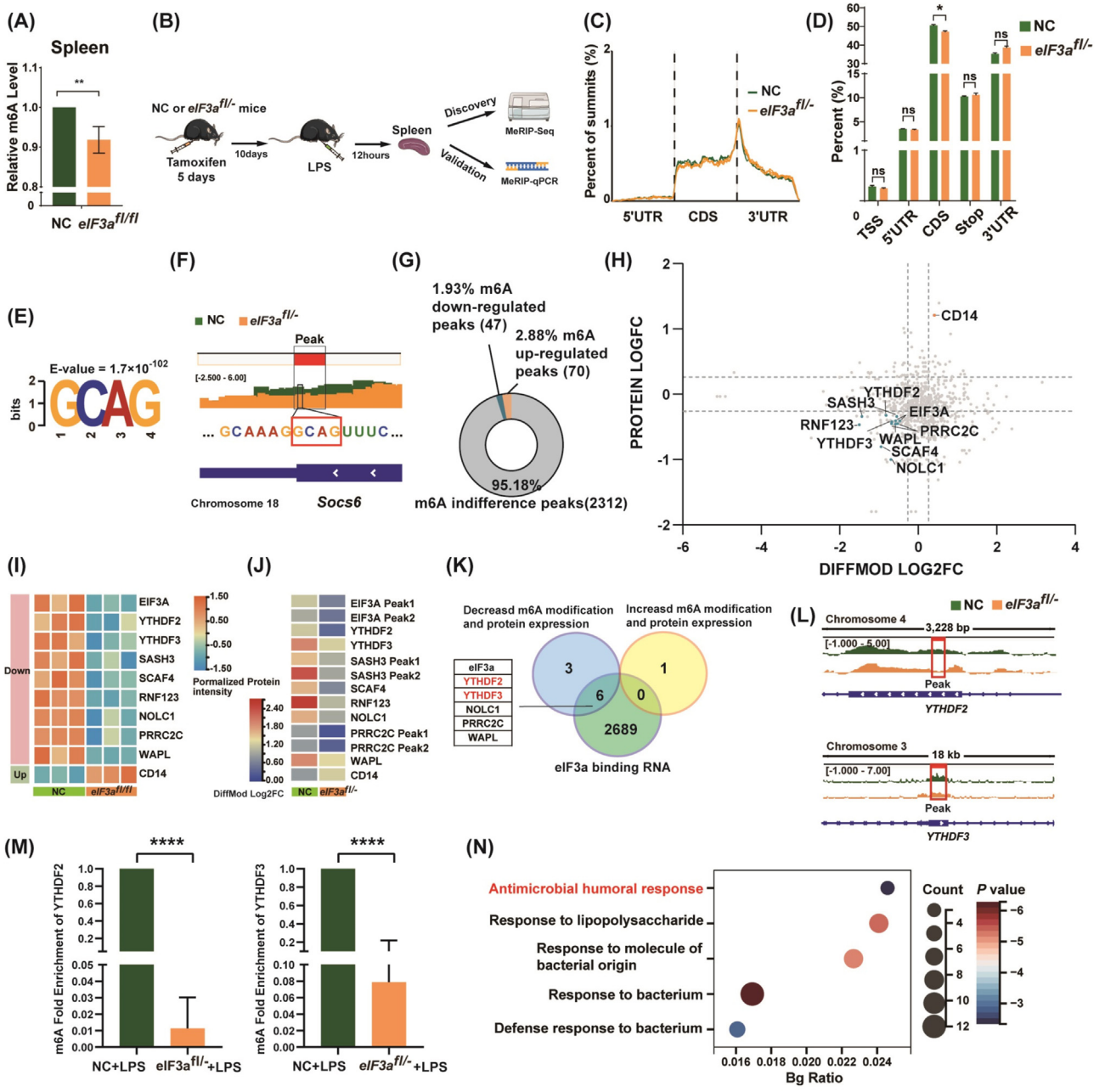

Figure 3 eIF3a regulates humoral immune response pathways *via* m^{6}A-mediated mechanisms. (A) Quantification of m^{6}A-modified mRNAs in the spleen of the *eIF3a*$^{fl/fl}$ and control mice. (B) Scheme of animal treatments and spleen isolation for MeRIP-seq and MeRIP-qPCR. (C, D) Distribution and proportion of m^{6}A modification in different positions (C) and regions (D) of mRNAs. (E, F) Putative motif for m^{6}A modification in mRNAs with higher frequency in *eIF3a*$^{fl/-}$ mice as compared to the control mice (E) and an example of such motif in an mRNA (F). (G) Changes in the population of mRNAs with m^{6}A modification in the *eIF3a*$^{fl/-}$ mice compared with the control animals. (H–J) Extract genes regulated in the same direction at the m^{6}A and protein levels. (H) The scatter plot reveals genes with significant differences (foldchange>1.2, *P* value < 0.05) at both the m^{6}A modification (horizontal axis) and protein (vertical axis) levels. The heatmap reveals the protein (I) and m^{6}A modification (J) levels of these genes in the two groups, respectively. (K) Overlaps between differential genes are shown in panel (J) and eIF3a binding RNA. (L) Peak plots of YTHDF2 and YTHDF3. (M) MeRIP-qPCR results of m^{6}A modification of YTHDF2 and YTHDF3 in B cells of septic *eIF3a*$^{fl/-}$ and control mice spleens. (N) Bacterial infected-related pathways enriched from genes that were upregulated at both the mRNA and protein levels. Data are presented as means ± SD ($n = 3$); *$P < 0.05$, **$P < 0.01$, ****$P < 0.0001$; ns, no significance.

and control mice were treated with tamoxifen for 5 days and 10 days after tamoxifen treatment, injected with LPS (Fig. 3B). Splenic RNA was then extracted at 12 h after LPS induction of sepsis and the differential m^{6}A modification was discovered by MeRIP-seq and validated by MeRIP-qPCR. After MeRIP-seq data processing and data quality control process, the Pearson's correlation test and Uniform Manifold Approximation and Projection(UMAP) plot revealed significant disparities between the control and *eIF3a*$^{fl/-}$ groups, while the intra-group differences were relatively minor (Supporting Information Fig. S6A−S6D), suggesting that the data quality is satisfactory. The m^{6}A-modified fragments were identified as the detected "peaks" in the analysis. There were no significant differences in the count and average enrichment between the two groups (Fig. S6E and S6F). The distribution of m^{6}A peaks on mRNA was found to be concentrated in the coding sequence (CDS) region and highest near termination codons (STOP) across all samples, which is consistent with previous reports[25] (Fig. 3C), indicating the reliability of our data. The average proportions of m^{6}A peaks located in the CDS relative to total m^{6}A modifications in the control and *eIF3a*$^{fl/-}$ mice were 50.63% and 47.18%, respectively (Fig. 3D). However, there is no change in the relative m^{6}A modifications in other regions. Thus, reduction in eIF3a expression may lead to decreased m^{6}A modification in the CDS but not other regions including 5′- or 3′-UTRs. A specific "RRACH" motif for m^{6}A modification was identified in both *eIF3a*$^{fl/-}$ and control mice. The "RRACH" motif is a well-recognized consensus sequence for m^{6}A modification. The breakdown of this motif is as follows: R = purine (adenine (A) or guanine (G)), R = purine (adenine (A) or guanine (G)), A = adenine (A), CH = any base (A, C, G or T/U). "RRACH" enriching indicates that the peaks analyzed in the data were m^{6}A-modified fragments, confirming the accuracy of the results (Fig. S6G). We also identified motifs "GCAG", which were more enriched in the control than the *eIF3a*$^{fl/-}$ mice (Fig. 3E and F), suggesting that these motifs may be specific to eIF3a regulation. To investigate whether m^{6}A modification affects mRNA expression, we examined the correlation between expression with peak intensity and regions. As shown in Fig. S6H−S6J, the reduction of eIF3a in *eIF3a*$^{fl/-}$ mice did not lead to changes in mRNA level through altered m^{6}A modification. Next, we calculated the overlapping peaks of m^{6}A between the two groups and their differences. There were 2429 overlapping peaks between the two groups, among which 2312 showed no significant difference. Of the remaining mRNAs, 70 were up-regulated and 47 were down-regulated in *eIF3a*$^{fl/-}$ mice (Fig. 3G).

Since the function of eIF3a as a reader is to initiate translation, the target of eIF3a should be affected in protein expression level. To investigate the protein expression of the differential m^{6}A-modified mRNAs, we integrated Merip-seq data and proteomic data. The differentially expressed proteins of *eIF3a*$^{fl/-}$ mice were intersected with differentially m^{6}A modified genes (Fig. 3H). The gene with both up-regulated m^{6}A modification level and protein expression was CD14. On the other hand, 9 genes showed down-regulated m^{6}A modification and protein expression level (EIF3A, YTHDF2, YTHDF3, SASH3, SCAF4, RNF123, NOLC1, PRR2C2 and WAPL) (Fig. 3I and J). These genes may be the ultimate functional targets of eIF3a through m^{6}A modification. To elucidate the underlying molecular mechanisms of eIF3a regulation m^{6}A modified mRNAs, it is imperative to identify the RNAs that specifically bind to eIF3a. By intersecting these 10 genes with eIF3a-binding mRNA set, we identified the targets directly bound by eIF3a. RNA immunoprecipitation sequencing (RIP-seq) is a widely used method to study protein-RNA interactions and detect RNA interactions with certain proteins. We analyzed publicly available eIF3a-RIP datasets (GSE65004, GSE73405, and RMBase websites) in comparison with our datasets. Of 2699 eIF3a-bound mRNAs in the eIF3a-RIP datasets, 6 were found in our genes with decreased mRNA m^{6}A modification and protein expression (Fig. 3K). Interestingly, we found that there are two m^{6}A readers among these genes, YTHDF2 and YTHDF3. The 2 peaks with the greatest differences were identified by mapping the peak discrepancies in these mRNAs (Fig. 3L).

To verify this result, we used flow cytometry to sort B cells from the spleens of *eIF3a*$^{fl/-}$ septic mice and control septic mice, and verified the difference in m^{6}A peaks of YTHDF2 and YTHDF3 through MeRIP-qPCR experiments. The results showed that the YTHDF2 m^{6}A modification in B cells of *eIF3a*$^{fl/-}$ mice was about 1%, and the YTHDF3 m^{6}A modification was 7% in the B cells of control mice, which was consistent with the MeRIP-seq analysis results (Fig. 3M). The function of YTHDF2 is to bind to m^{6}A-modified mRNA and promote its degradation, and the function of YTHDF3 is to assist YTHDF2 in its function. Therefore, the reduction of these 2 readers may lead to reduced degradation of their target RNA and increased expression of proteins coded by the target RNA. Genes that increased in *eIF3a*$^{fl/-}$ mice spleen in both RNA and protein levels were extracted and subjected to enrichment analysis. We found 5 enriched results related to bacterial infection (Fig. 3N). Among them, we noticed that some genes were enriched in the antimicrobial humoral response pathway. It is known that the main immune cells of humoral immunity are B cells, and B cells make up 60% of the white pulp in the spleen. These results provide a hint that eIF3a may play a crucial role in regulating B cell function.

Meanwhile, the results of flow analysis of mouse spleens showed that only B cells but not other cells were significantly different, and the proportion of B cells was lower in *eIF3a*$^{fl/-}$ mice than in NC mice (Fig. S2J and S2K). Therefore, we hypothesized that m^{6}A modification and expression differences may be related to the change in B cell proportion, and the difference in eIF3a is the cause of the change in B cell proportion. B cell dysfunction caused by upregulation of humoral immune response genes are mechanism leading to more severe sepsis in *eIF3a*$^{fl/-}$ mice. However, further *in vivo* experiments are needed to validate this hypothesis.

3.5. *eIF3a maintains the quantity and function of B cells*

In experiments exploring the effects of eIF3a on B cells, we used *eIF3a*$^{fl/fl}$ mice as the experimental group based on complete knockout of *eIF3a* in their spleens. We determined the number of B cells in the spleen and blood by determining B220 and CD19 as B cell markers using flow cytometry and immunofluorescence (Fig. 4A). Fig. 4B shows a significant reduction in spleen B cell population with 20% in the *eIF3a*$^{fl/fl}$ mice compared with 35% B cells in the control mice. Consistently, B cells in the white pulp are severely depleted in the *eIF3a*$^{fl/fl}$ mice with only 0.2% compared with the control mice with approximately 60% (Fig. 4C). Since B cells differentiate into effector B cells (plasma cells) in the spleen, we used flow cytometry to detect plasma cells. As shown in Fig. 4D, the *eIF3a*$^{fl/fl}$ mice had 5% plasma cells in their spleen compared to about 7% in the control mice. Thus, down-regulation of eIF3a expression decreases B cell population in spleen.

We next investigated the effect of *eIF3a* knockdown on B cell CDC function by examining production of anti-sheep red blood

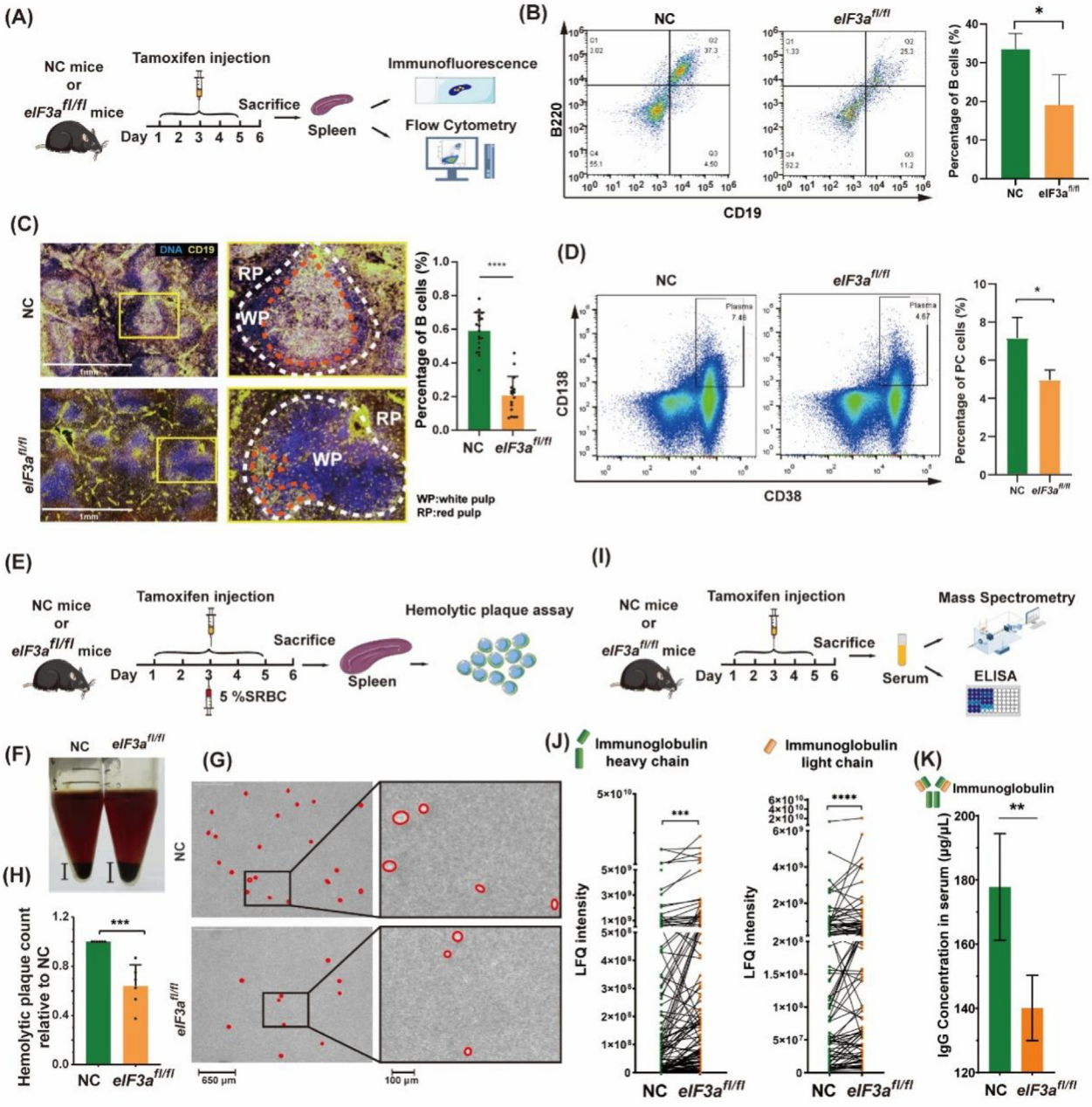

Figure 4 eIF3a regulation of B cell production and function. (A, E, I) Scheme of experimental design for quantification of B cells in the spleen (A), hemolytic plaque assay of SRBC using spleen (E), and quantification of IgG levels in the blood (I) from the control and *eIF3a*$^{fl/fl}$ mice. (B, C) B cell population in the spleen as determined by staining CD19 and CD220 and detected using flow cytometry (B) and immunofluorescence microscopy (C). White and orange circles in panel (C) indicate the white pulp (WP) and B cell regions, respectively. (D) Plasma cells in the control and *eIF3a*$^{fl/fl}$ mice as determined by staining CD38 and CD138 and detected using flow cytometry. (F–H) Immunogenic response of the control and *eIF3a*$^{fl/fl}$ mice to injected SRBC. The height of the SRBC precipitate (F) and the amount of hemolytic plaque (G, H) suggest the degree of SRBC hemolysis. Red circles in panel (G) mark the edges of the hemolytic plaques. Panel (H) represents quantification of the relative count of hemolytic plaques from panel (G). (J, K) Expression levels of immunoglobulin heavy and light chains in serum of the control and *eIF3a*$^{fl/fl}$ mice as determined using Mass Spectrometry (J) and intact IgG using ELISA (K). Data are presented as means ± SD ($n = 6$); $^{*}P < 0.05$, $^{**}P < 0.01$, $^{***}P < 0.001$, $^{****}P < 0.0001$.

cell (anti-SRBC) antibodies from mouse B cells in the *eIF3a*$^{fl/fl}$ mice using precipitation and hemolytic plaque assays (Fig. 4E). As shown in Fig. 4F, the *eIF3a*$^{fl/fl}$ mice had more SRBC precipitation than the control mice, indicating the presence of more intact SRBCs in the *eIF3a*$^{fl/fl}$ mice. This finding suggests a decreased ability of *eIF3a*$^{fl/fl}$ mice to produce specific anti-SRBC antibodies. Indeed, in the hemolytic plaque assay, the blood from the *eIF3a*$^{fl/fl}$ mice formed about 40% fewer plaques compared with

the control mice (Fig. 4G and H). Thus, the B cell function in the *eIF3a*$^{fl/fl}$ mice is likely impaired.

Finally, since immunoglobulins, which consist of light and heavy chains, are the main effectors of B-cell function, we quantified serum light and heavy chains using mass spectrometry and intact IgG using ELISA of both the *eIF3a*$^{fl/fl}$ and control mice (Fig. 4I). As shown in Fig. 4J, the levels of both serum light and heavy chains were higher in the *eIF3a*$^{fl/fl}$ mice than in the control mice. However, the level of serum intact IgG antibodies in the *eIF3a*$^{fl/fl}$ mice is significantly less than in the control mice (Fig. 4K). These results indicate that intact immunoglobulins are reduced and immunoglobulin light and heavy chains are increased in the serum of *eIF3a*$^{fl/fl}$ mice. It is hypothesized that these results may be responsible for the reduced immunity of *eIF3a*$^{fl/fl}$ mice and the onset of severe systemic inflammatory responses, possibly caused by apoptotic B cells.

According to these results, the degree of eIF3a reduction is related to the degree of B cell activation. The B cells of heterozygous knockout *eIF3a* mice are mildly activated, mainly proliferating. However, the B cells of homozygous knockout mice are overactivated and inhibited. The reduction of eIF3a makes mice more likely to reach overactivation and inhibition, thus *eIF3a* knockout mice are more susceptible to severe sepsis than wild-type mice. Taken together, the reduction of eIF3a expression may deplete B cells and impair their functions, contributing to severe sepsis after infection, which represents a novel mechanism underlying the systemic inflammatory response in sepsis.

3.6. *Association of eIF3a with B cell quantity and function in sepsis patients*

To determine the clinical implication of eIF3a expression in systemic inflammatory response, we analyzed the relationship between eIF3a expression and B cell function in sepsis patients compared with healthy individuals. Three datasets were collected from GEO database, consisting of PBMC samples from both healthy individuals and sepsis patients. Firstly, to explore the difference in B cell function and quantity between healthy individuals and sepsis patients, the abundance of B cell states within them was analyzed using Ecotyper software. B cells have five distinct functional and differentiation states, namely CD53$^+$ activated, IKBKB + activated, unswitched memory, exhausted memory, and naive B cells. As shown in Fig. 5A, there was a significant decrease in total B cell abundance among septic patients compared to healthy individuals. Among these B cells, the reduction of the naive and CD53$^+$ activated B cells in sepsis patients was particularly evident compared with healthy individuals (Fig. 5B).

We next determined eIF3a expression in both sepsis and healthy patients. Because eIF3a has been shown to regulate m^{6}A, we also analyzed and compared with 7 other known sepsis-related m^{6}A regulators (METTL3, METTL14, ALKBH5, FTO, YTHDF1, YTHDF2, and YTHDF3) for comparison. As shown in Fig. 5C, among these 8 m^{6}A regulators, only eIF3a showed a consistent dramatic reduction in sepsis patients across the three datasets. To validate this result, we induced sepsis in mice using LPS and measured the expression of eIF3a in the spleen. The results showed a significant decrease in eIF3a expression in mice after LPS treatment, which aligns with the RNA-seq findings (Fig. S5D). Association analysis of eIF3a expression with the abundance of naive and CD53$^+$ activated B cells showed significant positive correlations in these datasets analyzed (Fig. 5D). We used LPS-induced septic mice to validate the relationship between eIF3a expression and B cell ratio at single-cell resolution. *eIF3a*$^{fl/-}$ mice and NC mice were both assayed for splenic B cell ratios by flow cytometry 12 h after LPS injection. The results showed that the B cell ratio of *eIF3a*$^{fl/-}$+LPS mice was significantly lower than that of control + LPS mice, and the B cell ratio of both groups was lower than that of mice without LPS treatment (Fig. 5E, Fig. S2J). Thus, reduced eIF3a expression may lead to a reduction in B cells and an increased risk of sepsis. Additionally, we individually calculated the differential expressed genes between eIF3a-H and eIF3a-L across the three datasets and obtained a total of 213 upregulated genes and 0 downregulated genes through their intersection. We performed enrichment analysis on the upregulated genes, and the results indicate that the genes enriched in the eIF3a-H group, which exhibit high expression, are involved in the regulation of B cell proliferation and activation. This suggests that eIF3a may regulate the quantity and function of B cells in septic patients (Fig. 5F).

We also analyzed scRNA sequencing data of PBMCs to determine B cell function in patients with different levels of eIF3a expression. After filtering the data, we performed a two-dimensional tSNE projection and created a chart showing the expression of cell markers in each cluster (Fig. 5G, Supporting Information Fig. S7). Four sepsis patients were categorized into B cell high (eIF3a-H) and low (eIF3a-L) eIF3a expressers (Fig. 5H). Differential genes between the eIF3a-H and eIF3a-L groups of B cells were calculated and subjected to enrichment analysis (Fig. 5I). We found that both upregulated and downregulated genes in the eIF3a-H group were involved in B cell-related pathways. Specifically, the downregulated genes were primarily associated with the BCR signaling pathway and activation of NF-κB in B cells pathway, which may prevent excessive BCR signaling activation and inflammatory responses. On the other hand, the upregulated genes were mainly enriched in immunoglobulin formation, suggesting that the eIF3a-H group may have enhanced specific immune function. For example, low expression of CD70 can prevent IFN-γ-mediated deletion of B cells[26]. CCR6 is reduced after B cell antigen receptor triggering and remains absent during differentiation into immunoglobulin-secreting plasma cells. Therefore, low expression of CCR6 may indicate stronger immunoglobulin secretion[27] (Fig. 5J). On the contrary, CD127 encoded IL-7R is beneficial for the survival and proliferation of B lymphocytes, while Tbx21 is crucial for the generation of effector B cells[28,29] (Fig. 5K). High expression of these two genes implies a larger number of B cells and stronger functionality. Based on the above findings, we conclude that B cells in patients with lower eIF3a levels may have a reduced ability to proliferate and differentiate, making it difficult to produce effective humoral immunity, leading to the development of severe sepsis. These findings are consistent with our above findings using animal models.

3.7. *eIF3a as a promising therapeutic strategy for sepsis*

To investigate the potential of using eIF3a as a strategy to treat sepsis, we performed a rescue experiment by over-expressing eIF3a in *eIF3a*$^{fl/-}$ mice. Firstly, we detected the efficiency and duration of ectopic eIF3a over-expression by injecting a plasmid for over-expression or a control empty vector into the tail vein of *eIF3a*$^{fl/-}$ mice (abbreviated as OE-*eIF3a*$^{fl/-}$ and Vec-*eIF3a*$^{fl/-}$ mice, respectively) followed by assessing eIF3a protein level in both mice. As shown in Fig. 6A and Supporting Information Fig. S8A, significant up-regulation of eIF3a expression in OE-

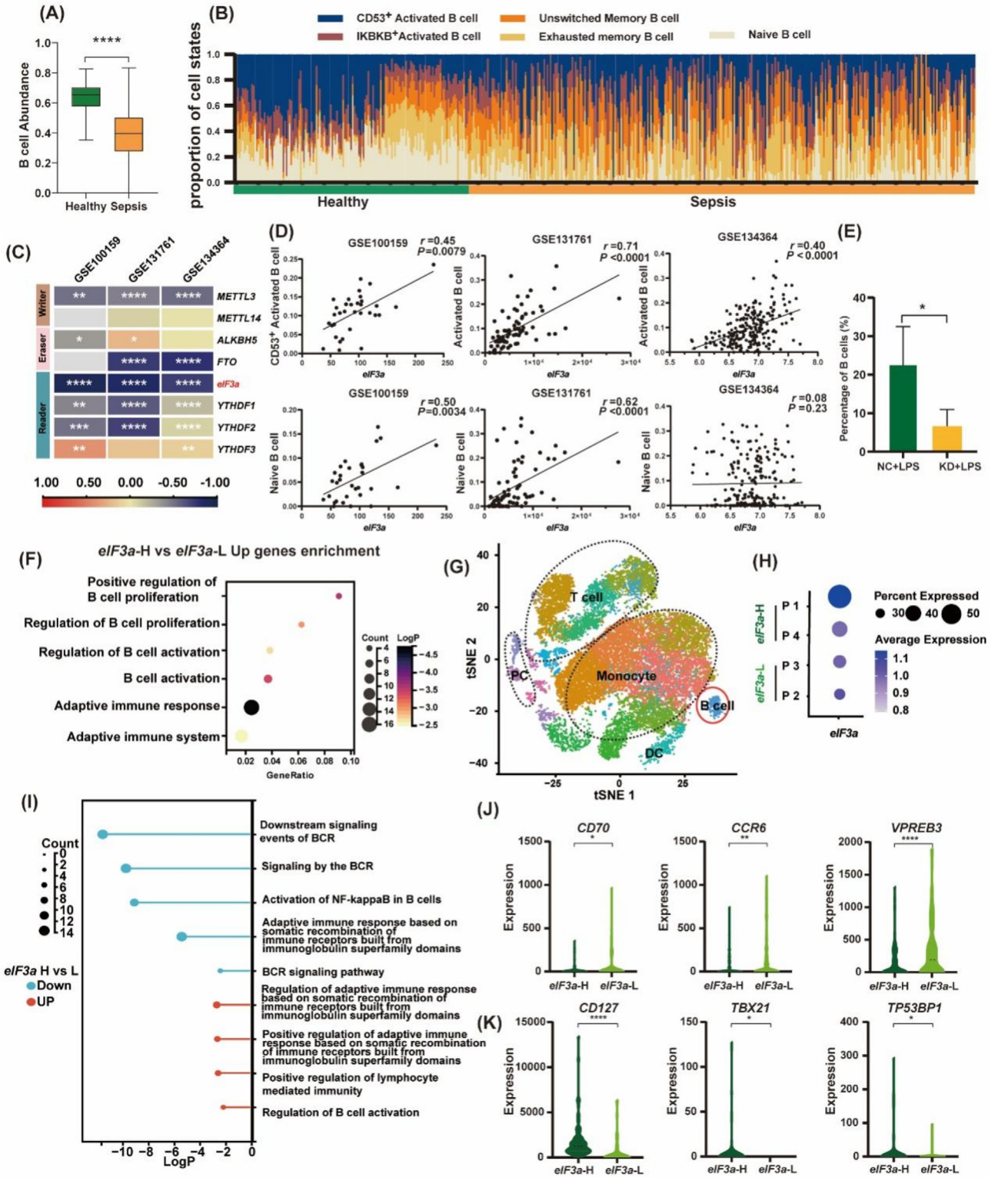

Figure 5 eIF3a expression and B cell quantity and function in septic patients. (A, B) Distribution of total (A) and types of B cells (B) in healthy individuals and septic patients. (C) Heat map displaying a differential expression of m^6A regulators between sepsis and healthy individuals of three datasets. (D) Spearman correlation between eIF3a expression and levels of different B cell types in three datasets. (E) B cell population in the spleen of LPS treated *eIF3a*$^{fl/-}$ and control mice was determined by staining CD19 and CD220 and detected using flow cytometry. (F) Enrichment analysis of the intersection genes with higher expression in eIF3a-H compared to eIF3a-L across the three datasets. (G) tSNE plot of all patients scRNA-seq data. (H) Patients were classified into eIF3a-H and eIF3a-L groups based on the expression of eIF3a in B cells. (I) Enrichment analysis revealed upregulated and downregulated B cell related pathways in eIF3a-H relative to eIF3a-L. (J, K) Expression of CD70, CCR6, VPREB3, CD127, TBX21 and TP53BP1 in B cells of eIF3a-L and eIF3a-H septic patients. Data are presented as means ± SD ($n = 3$); $^*P < 0.05$, $^{**}P < 0.01$, $^{****}P < 0.0001$.

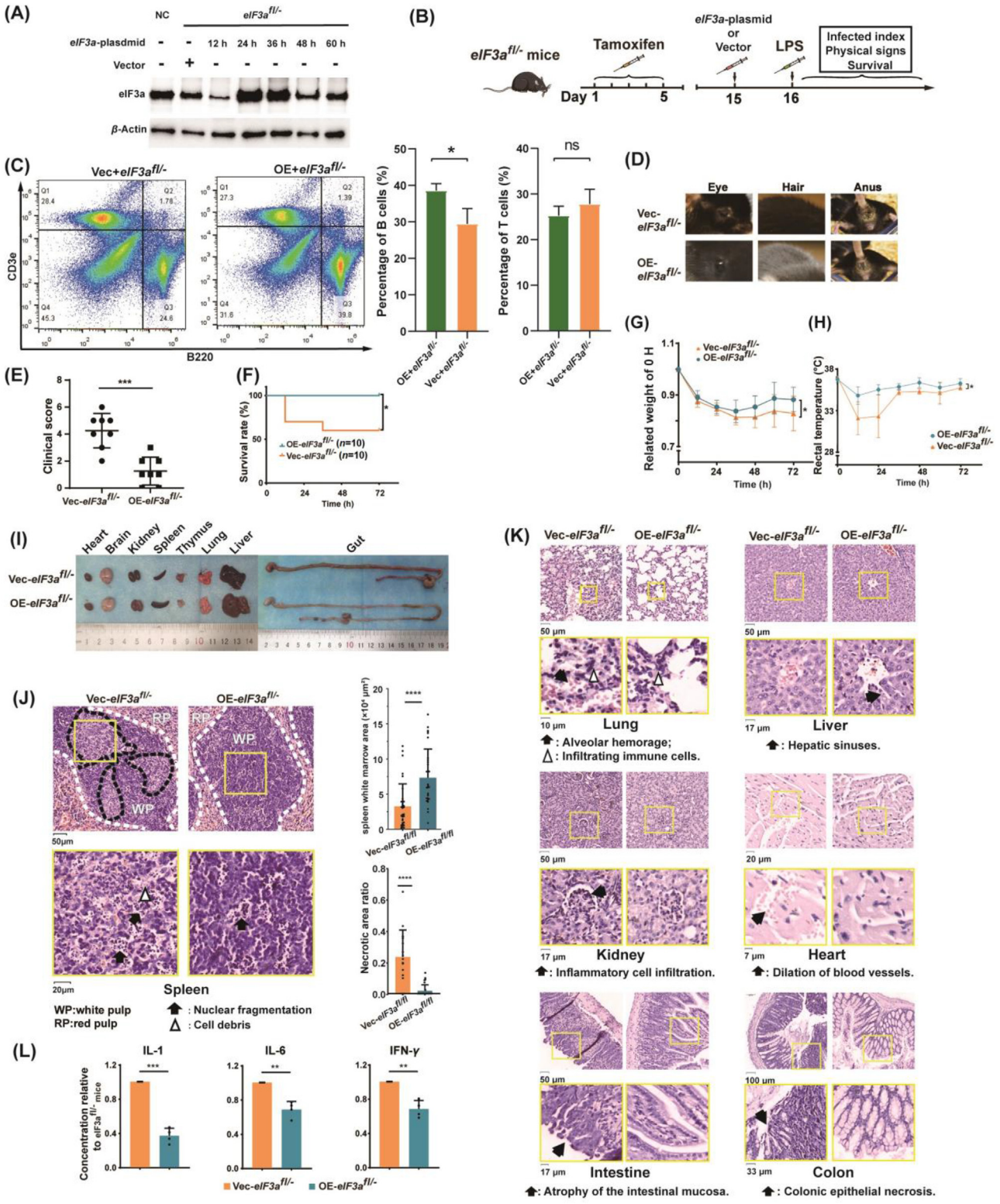

Figure 6 Ectopic eIF3a overexpression protects against LPS-induced inflammation and severe sepsis in the *eIF3a*$^{fl/-}$ mice. (A) Western blot of eIF3a in the *eIF3a*$^{fl/-}$ mice injected with plasmid for ectopic eIF3a overexpression or empty vector. (B) Flow cytometry was performed to detect the proportions of B cells and T cells in the spleen, and the quantification results are shown on the right. (C) Scheme of the *eIF3a* knockdown, ectopic overexpression and LPS induction of sepsis. (D−H) Status of eye, hair, and anus (D) and clinical scores of sepsis at 24 h (E), overall survival rate (F), body weight (G) and rectal temperature (H) of the mice over 72 h following LPS injection. (I) Gross anatomy of major organs in the OE-*eIF3a*$^{fl/-}$ and Vec-*eIF3a*$^{fl/-}$ mice after sepsis induction. (J, K) Images of HE-stained sections of the spleen (J) and other organs (K) of the OE-*eIF3a*$^{fl/-}$ and Vec-*eIF3a*$^{fl/-}$ mice. A quantified white pulp area in the spleen was presented in the histogram. (L) The relative concentration of IL-1, IL-6, and IFN-γ in serum at 24 h after LPS injection. Data are presented as means ± SD ($n = 8$); $^{*}P < 0.05$, $^{**}P < 0.01$, $^{***}P < 0.001$, $^{****}P < 0.0001$.

eIF3a$^{fl/-}$ mice was found at 24−36 h after injection, surpassing that of NC and Vec-*eIF3a*$^{fl/-}$ mice. We examined the proportions of B cells and T cells in the spleen of both mouse groups. As shown in Fig. 6B, the spleen B cell percentage in OE-*eIF3a*$^{fl/-}$ mice reached 37%, significantly higher than the 29% observed in Vec-*eIF3a*$^{fl/-}$ mice. There were no significant changes in T cell proportions.

Therefore, we speculate that OE-*eIF3a*$^{fl/-}$ mice may exhibit enhanced resistance to LPS. Thus, we used this model to investigate the protective effect of eIF3a overexpression against sepsis. To ensure the high expression level of eIF3a during LPS induction of sepsis, LPS injection was performed 24 h after injection of the plasmid (Fig. 6C). As expected, the OE-*eIF3a*$^{fl/-}$ group did not exhibit significant sepsis, while the control Vec-*eIF3a*$^{fl/-}$ mice developed severe orbital secretions, hair erection, and diarrhea (Fig. 6D). All OE-*eIF3a*$^{fl/-}$ mice had low clinical scores, indicating the absence of severe sepsis (Fig. 6E). Survival analyses showed that all OE-*eIF3a*$^{fl/-}$ mice were alive, while Vec-*eIF3a*$^{fl/-}$ mice had a 50% mortality rate at 72 h after LPS injection (Fig. 6F). Additionally, the OE-*eIF3a*$^{fl/-}$ mice exhibited less weight loss compared to the Vec-*eIF3a*$^{fl/-}$ mice (Fig. 6G). The Vec-*eIF3a*$^{fl/-}$ mice had more severe hypothermia compared to the OE-*eIF3a*$^{fl/-}$ mice, which began to recover within 24 h following LPS infection (Fig. 6H). These results suggest that eIF3a overexpression protects mice from severe sepsis after LPS infection.

Next, the protective efficacy of eIF3a against inflammation in internal organs was evaluated. Gross anatomy analyses revealed a significant increase in spleen size in the OE-*eIF3a*$^{fl/-}$ mice compared to the Vec-*eIF3a*$^{fl/-}$ mice. In contrast to pulmonary hemorrhage, liver congestion or intestinal dilatation in the Vec-*eIF3a*$^{fl/-}$ mice, the OE-*eIF3a*$^{fl/-}$ mice showed no significant signs of organ abnormalities (Fig. 6I). Histologically, the loss of white pulp area in the spleen due to *eIF3a* knockdown (see above) was recovered as shown by approximately 2-fold increase of white pulp area in the OE-*eIF3a*$^{fl/-}$ mice compared to Vec-*eIF3a*$^{fl/-}$ mice (Fig. 6J). In addition, there were patchy necrotic regions (black dotted line) with nucleus crumple, cytoplasmic debris, and infiltration of red blood cells in the white pulp of Vec-*eIF3a*$^{fl/-}$ mice, whereas the white pulp in the OE-*eIF3a*$^{fl/-}$ mice has less patchy necrosis but instead with a “starry sign” of spotty necrosis. The average necrotic area ratio in the white pulp of the OE-*eIF3a*$^{fl/-}$ mice was estimated to be 0.02, about 11 times less than that in the control Vec-*eIF3a*$^{fl/-}$ mice with a ratio of 0.23 (Fig. 6J). Together, these results suggest that eIF3a over-expression can rescue its knockdown-induced inflammatory injury in the white pulp in the spleen during sepsis.

The protection against LPS-induced inflammation by eIF3a overexpression was also observed in other organs. As shown in Fig. 6K, less extensive alveolar atrophy, hemorrhage, and inflammatory cell infiltration were observed in the lungs of the OE-*eIF3a*$^{fl/-}$ mice compared with the Vec-*eIF3a*$^{fl/-}$ mice. In the livers of these mice, clear hepatic sinusoids remained in the OE-*eIF3a*$^{fl/-}$ mice. In contrast, there is extensive hepatocellular edema and disappearance of hepatic sinusoids in the Vec-*eIF3a*$^{fl/-}$ mice. The kidneys of the Vec-*eIF3a*$^{fl/-}$ mice had significant inflammatory cell infiltration in the glomeruli, which is absent in the OE-*eIF3a*$^{fl/-}$ mice. The blood vessels in the hearts were dilated in the Vec-*eIF3a*$^{fl/-}$ mice but not in the OE-*eIF3a*$^{fl/-}$ mice. The mucosa in the intestines and colons of the Vec-*eIF3a*$^{fl/-}$ mice had atrophy and necrosis, respectively, but was normal in the OE-*eIF3a*$^{fl/-}$ mice. These findings are consistent with the reduction of inflammatory factors including IL-1, IL-6, and INF-γ in these organs (Fig. S8B) and the serum (Fig. 6L) of the OE-*eIF3a*$^{fl/-}$ mice compared with the Vec-*eIF3a*$^{fl/-}$ mice. These findings suggest that overexpressing eIF3a in the *eIF3a*$^{fl/-}$ mice protects against LPS-induced severe inflammation and sepsis due to *eIF3a* knockdown, resulting in milder symptoms, faster recovery time, and reduced mortality rates. Finally, we injected the eIF3a overexpression plasmid into wild-type mice (OE + WT) and compared them with mice injected with the control plasmid (Vec + WT) (Fig. S8C). Similarly, the results showed that OE + WT mice had less weight loss, lower body temperature reduction, and a lower mortality rate compared to Vec + WT mice (0% *vs* 50%). Based on the comprehensive results, we conclude that supplementation of eIF3a can significantly enhance the resistance of mice to sepsis.

4. Discussion

In this study, we show that eIF3a deletion activates the systemic inflammatory response, resulting in severe LPS-induced sepsis in mouse models, and that restoring eIF3a expression rescues eIF3a deletion-induced sepsis. We also show that clinically low levels of eIF3a expression are associated with the severity of sepsis in sepsis patients. Furthermore, eIF3a maintains B cell quantity and function *via* regulating m^{6}A-modified mRNAs, which likely mediates inflammatory response and contribution of *eIF3a*-knockdown to LPS-induced sepsis. These findings provide a novel mechanism of B cell regulation in the development of sepsis and suggest that eIF3a may be developed as a strategy for treating sepsis.

Sepsis is a quick dysregulated host response to infection that results in multi-organ dysfunctions. These organs contain the heart, lung, liver, kidney, digestive tract, and skin. A global statistical report estimated nearly 50 million cases of sepsis every year[30]. Although sepsis mortality rates are gradually decreasing each year as treatment and care techniques improve, there are still approximately 11 million sepsis-related deaths, representing ∼20% of all deaths worldwide[30]. Previously, it was thought that organ dysfunction is due to imbalanced activation of pro-inflammatory response to infections[31] or anti-inflammatory response from an impaired immune system[32]. The main treatments of sepsis are antimicrobial therapy, source control, fluid resuscitation, and multiple organ support therapies though with limited prognostic impact[33-36]. For many years, the research and development of new drugs for sepsis has been in an unsatisfactory state. Certain medications have been developed to enhance immune function by regulating factors such as GM-CSF and protein C. However, their efficacy remains limited[37-40]. The fact that overexpressing eIF3a could make the mice suffering LPS-induced sepsis recover faster and reduce mortality rate suggests that strategies to increase eIF3a expression hold promise for sepsis treatments.

As an important component of adaptive immunity, B cells produce characteristic immunoglobulin repertoires during systemic infections[41,42]. However, the role of B cells in sepsis and their regulatory mechanisms are not well understood. While the immunoglobulins are mainly stored in memory and plasma cells, inactivated B cells receive antigenic stimuli through the lymphatic circulation, and then they are activated to produce specific antibodies[43]. This process is accomplished in secondary lymphoid structures, mainly in the spleen[44], which may be an important immune mechanism by which B cells prevent the development of sepsis. It is, thus, tempting to speculate that when the quantity and function of B cells are suppressed, more severe sepsis will develop

upon infection due to impaired humoral immunity. Indeed, the PBMC data analysis showed significant inhibition of B cell activation and proliferation capacity in septic patients and *eIF3a*$^{fl/-}$ mice with B cell impairment exhibited increased susceptibility to severe sepsis. B cells in septic shock patients have also been reported to present an exhausted-like/immunoregulatory profile[45,46]. Thus, suppression of B cells may be critical in the development of sepsis. Based on all the results, we speculate that the deficiency of eIF3a may lead to excessive activation of B cells, resulting in the production of a large number of inflammatory factors. Consequently, this inhibits the proliferation of B cells, impairs their ability to generate specific antibody responses, and promotes apoptosis.

It is worth noting that eIF3a is distinct from other m^{6}A readers as it triggers m^{6}A-mediated cap-independent translation[12]. During infection, eIF4E is inhibited, resulting in suppression of cap-dependent translation initiation[13]. In this case, cap-independent translation is essential for preserving cellular function. Based on the findings in this study, we conclude that eIF3a regulation of translation through m^{6}A during infection plays a crucial role in preventing severe sepsis. This implies that up-regulation of eIF3a expression may be an effective therapeutic strategy for sepsis. Currently, the septic drug discovery and development solely focus on targeting neutrophils, macrophages, and T cells[34,47], possibly because the roles and functions of other cells in sepsis are not well defined. As discussed above, we have uncovered a novel mechanism by which B cells contribute to sepsis resistance, potentially paving the way for groundbreaking advancements in sepsis treatment in the future. Sepsis is caused by a variety of immune cells and a variety of proteins, thus drugs targeting a single immune cell or a downstream protein have limited efficacy. Our MeRIP-seq and RNA-seq results demonstrate that eIF3a suppresses inflammation by regulating multiple pathways, including acquired immunity. Therefore, eIF3a may be a master regulator, and targeting eIF3a may offer improved efficacy.

The m^{6}A modification is widely distributed throughout mRNA and serves as a crucial mechanism for regulating gene expression, thus highlighting the pivotal role of m^{6}A regulators in this process[48]. Epi-omics is gradually being extended from mechanism research to clinical application[49]. One promising avenue is to explore regulation of m^{6}A modification, which has recently emerged as a key player in sepsis[50-53]. ALKBH5 enhances the intrinsic migratory capacity of neutrophils, thereby playing a role in antibacterial innate defense[51]. In sepsis, the up-regulation of METTL3 by neutrophil extracellular traps (NETs) may trigger alveolar epithelial cell ferroptosis through m^{6}A regulation, ultimately resulting in sepsis-associated acute lung injury[54]. Expression of METTL14 in macrophages exacerbates the production of cytokines and myocardial injury during sepsis[53]. Additionally, several factors have been reported to modulate the development and prognosis of sepsis through m^{6}A regulation[52,53]. In the current study, eIF3a may exert bidirectional control over sepsis by decreasing YTHDF2 and YTHDF3 expression to regulate humoral immune response. However, additional studies are clearly needed to validate these regulatory mechanisms.

The regulation of protein synthesis primarily occurs at the initiation step, enabling swift, reversible, and spatial control over gene expression[55]. The process necessitates a minimum of 9 eukaryotic initiation factors (eIFs)[5]. Although current research has investigated the specific roles of individual eIFs in mRNA translation, the physiological or pathological significance resulting from their loss remains unclear. Hence, it is imperative to conduct a comprehensive investigation of the function by utilizing whole-body knockout mice. To date, knockout mouse models have been engineered targeting only eIF2A and eIF4B, specifically impacting the nervous and immune systems in mice[56,57]. The *eIF3a* knockout mouse reported here represented the pioneering model for gene editing of eIF3a, significantly deepening our understanding of the pivotal functions of eIF3a and eIF protein family *in vivo*. From studies of this model, we have identified the paramount role of eIF3a in the immune system and its implication for sepsis treatments. It is noteworthy that previous studies of the *eIF4B* knockout mouse demonstrated similar phenotypes in the immune system, suggesting that the *eIF* genes and translational control of gene expression may play a crucial role in physiological function, particularly within the immune system[56].

It is worth noting that eIF3a is a core component of the eIF3 complex and plays a critical role in the regulation of global protein synthesis and cell signaling pathways. Disruption of eIF3a could therefore have wide-ranging effects on cellular homeostasis and physiology. On the one hand, immune system is a complex, interconnected network of different cell types. Thus, in addition to B cells, other cell types may also play important roles. On the other hand, the absence of eIF3a may have detrimental effects on different tissue cells beyond inflammation, as observed in the impaired sperm development in *eIF3a*$^{fl/fl}$ mice. These tissue damages, along with immune system abnormalities, may collectively contribute to the formation of a susceptible mechanism for sepsis. The limited number of sepsis patient scRNA-seq samples in this study has restricted the exploration of the association between eIF3a and B cells in sepsis. In future research, increased clinical sample size and more in-depth mechanistic investigations would be beneficial for further understanding the significance of eIF3a in sepsis. These advancements would provide a deeper insight into the role of eIF3a in sepsis and its potential implications.

5. Conclusions

In summary, using *eIF3a* knockout model we have revealed a new signaling axis in sepsis development involving eIF3a and m^{6}A regulation of B cell production and function. Moreover, eIF3a may be used for development of therapeutic strategies for sepsis.

Acknowledgments

This work was supported by the National Natural Science Foundation of China (82450103, 82373962, 82073943 to Jiye Yin, and 82173901 to Zhaoqian Liu, 82204533 to Jiajia Cui), Scientific research project of Furong laboratory of Central South University (No. 2023SK2083, China), The Natural Science Foundation of Hunan Province of China (2023JJ40931 to Jiajia Cui, 2023JJ30822 to Chengxian Guo, 2024JJ6633 to Yang Wang, 2021JJ30428, 2024JJ8180 to Juan Chen, 2024JJ9245 to Cenhui Luo, 2021JJ80087 to Liansheng Wang), Major Project of Natural Science Foundation of Hunan Province of China (Open competition, 2021 JC0002 to Zhaoqian Liu), Hunan Province key research and development plan of China (2023SK2007 to Zhaoqian Liu), Science and Technology Program of Changsha of China (kh2003010 to Zhaoqian Liu), the Wisdom Accumulation and Talent Cultivation Project of the Third Xiangya Hospital of Central South University (YX202110 to Chengxian Guo, China),

China Postdoctoral Science Foundation (2023M733973 to Juan Chen) and the Hunan Cancer Hospital Climb Plan (YF2020011 to Chenhui Luo, China), Health Research Project of Hunan Provincial Health Commission (B202305017863 to Chenhui Luo, China), the Association Foundation Program of Yunnan Provincial Science and Technology Department and Kunming Medical University (202001AY070001-282 to Jianming Xia, China). Open Fund of Shenzhen Key Laboratory of Chinese Medicine Active Substance Screening and Translational Research (ZDSYS20220606100801003 to Jiajia Cui, China). The Postdoctoral Fellowship Program of CPSF (GZB20240878 to Yang Wang, China). This work was partially supported by the High Performance Computing Center of Central South University.

Author contributions

Qianying Ouyang: Writing − original draft, Resources, Investigation, Formal analysis, Data curation. Jiajia Cui: Methodology. Yang Wang, Ke Liu: Software, Methodology. Yan Zhan: Software, Methodology. Wei Zhuo: Resources. Juan Chen: Resources. Honghao Zhou: Resources. Chenhui Luo: Software. Jianming Xia: Resources. Liansheng Wang: Methodology. Chengxian Guo: Formal analysis. Jianting Zhang: Writing − review & editing. Zhaoqian Liu: Project administration. Jiye Yin: Supervision, Project administration, Funding acquisition, Conceptualization.

Conflicts of interest

The authors declare no conflicts of interest.

Appendix A. Supporting information

Supporting information to this article can be found online at https://doi.org/10.1016/j.apsb.2025.02.005.

References

1. Das S, Vera M, Gandin V, Singer RH, Tutucci E. Intracellular mRNA transport and localized translation. *Nat Rev Mol Cell Biol* 2021;**22**:483−504.
2. Tahmasebi S, Khoutorsky A, Mathews MB, Sonenberg N. Translation deregulation in human disease. *Nat Rev Mol Cell Biol* 2018;**19**:791−807.
3. Browning KS, Gallie DR, Hershey JW, Hinnebusch AG, Maitra U, Merrick WC, et al. Unified nomenclature for the subunits of eukaryotic initiation factor 3. *Trends Biochem Sci* 2001;**26**:284.
4. des Georges A, Dhote V, Kuhn L, Hellen CU, Pestova TV, Frank J, et al. Structure of mammalian eIF3 in the context of the 43S preinitiation complex. *Nature* 2015;**525**:491−5.
5. Yin JY, Zhang JT, Zhang W, Zhou HH, Liu ZQ. eIF3a: a new anticancer drug target in the eIF family. *Cancer Lett* 2018;**412**:81−7.
6. Yin JY, Meng XG, Qian CY, Li XP, Chen J, Zheng Y, et al. Association of positively selected eIF3a polymorphisms with toxicity of platinum-based chemotherapy in NSCLC patients. *Acta Pharmacol Sin* 2015;**36**:375−84.
7. Yin JY, Dong ZZ, Liu RY, Chen J, Liu ZQ, Zhang JT. Translational regulation of RPA2 *via* internal ribosomal entry site and by eIF3a. *Carcinogenesis* 2013;**34**:1224−31.
8. Ma S, Dong Z, Huang Y, Liu JY, Zhang JT. eIF3a regulation of mTOR signaling and translational control *via* HuR in cellular response to DNA damage. *Oncogene* 2022;**41**:2431−43.
9. Yin JY, Shen J, Dong ZZ, Huang Q, Zhong MZ, Feng DY, et al. Effect of eIF3a on response of lung cancer patients to platinum-based chemotherapy by regulating DNA repair. *Clin Cancer Res* 2011;**17**:4600−9.
10. Liu RY, Dong Z, Liu J, Yin JY, Zhou L, Wu X, et al. Role of eIF3a in regulating cisplatin sensitivity and in translational control of nucleotide excision repair of nasopharyngeal carcinoma. *Oncogene* 2011;**30**:4814−23.
11. Chen YX, Wang CJ, Xiao DS, He BM, Li M, Yi XP, et al. eIF3a R803K mutation mediates chemotherapy resistance by inducing cellular senescence in small cell lung cancer. *Pharmacol Res* 2021;**174**:105934.
12. Meyer KD, Patil DP, Zhou J, Zinoviev A, Skabkin MA, Elemento O, et al. 5′ UTR m^{6}A promotes Cap-independent translation. *Cell* 2015;**163**:999−1010.
13. Lee AS, Kranzusch PJ, Doudna JA, Cate JH. eIF3d is an mRNA cap-binding protein that is required for specialized translation initiation. *Nature* 2016;**536**:96−9.
14. Hwang SY, Jung H, Mun S, Lee S, Park K, Baek SC, et al. L1 retrotransposons exploit RNA m^{6}A modification as an evolutionary driving force. *Nat Commun* 2021;**12**:880.
15. Elbarbary RA, Lucas BA, Maquat LE. Retrotransposons as regulators of gene expression. *Science* 2016;**351**:aac7247.
16. Su R, Dong L, Li Y, Gao M, He PC, Liu W, et al. METTL16 exerts an m^{6}A-independent function to facilitate translation and tumorigenesis. *Nat Cell Biol* 2022;**24**:205−16.
17. Tatomer DC, Wilusz JE. An unchartered journey for ribosomes: circumnavigating circular RNAs to produce proteins. *Mol Cell* 2017;**66**:1−2.
18. Zhuo W, Chen J, Jiang S, Zheng J, Huang H, Xie P, et al. Proteomic profiling of *eIF3a* conditional knockout mice. *Front Mol Biosci* 2023;**10**:1160063.
19. Gobbetti T, Coldewey SM, Chen J, McArthur S, le Faouder P, Cenac N, et al. Nonredundant protective properties of FPR2/ALX in polymicrobial murine sepsis. *Proc Natl Acad Sci U S A* 2014;**111**:18685−90.
20. Dong Q, Yan X, Liang Y, Stein SE. In-depth characterization and spectral library building of glycopeptides in the tryptic digest of a monoclonal antibody using 1D and 2D LC−MS/MS. *J Proteome Res* 2016;**15**:1472−86.
21. Liu Q, Gregory RI. RNAmod: an integrated system for the annotation of mRNA modifications. *Nucleic Acids Res* 2019;**47**:W548−55.
22. Tang Y, Chen K, Song B, Ma J, Wu X, Xu Q, et al. m^{6}A-Atlas: a comprehensive knowledgebase for unraveling the *N*^{6}-methyladenosine (m^{6}A) epitranscriptome. *Nucleic Acids Res* 2021;**49**:D134−43.
23. Luca BA, Steen CB, Matusiak M, Azizi A, Varma S, Zhu C, et al. Atlas of clinically distinct cell states and ecosystems across human solid tumors. *Cell* 2021;**184**:5482-96.e28.
24. Zhou Y, Zhou B, Pache L, Chang M, Khodabakhshi AH, Tanaseichuk O, et al. Metascape provides a biologist-oriented resource for the analysis of systems-level datasets. *Nat Commun* 2019;**10**:1523.
25. Meyer KD, Saletore Y, Zumbo P, Elemento O, Mason CE, Jaffrey SR. Comprehensive analysis of mRNA methylation reveals enrichment in 3′ UTRs and near stop codons. *Cell* 2012;**149**:1635−46.
26. Arens R, Tesselaar K, Baars PA, van Schijndel GM, Hendriks J, Pals ST, et al. Constitutive CD27/CD70 interaction induces expansion of effector-type T cells and results in IFNgamma-mediated B cell depletion. *Immunity* 2001;**15**:801−12.
27. Krzysiek R, Lefevre EA, Bernard J, Foussat A, Galanaud P, Louache F, et al. Regulation of CCR6 chemokine receptor expression and responsiveness to macrophage inflammatory protein-3alpha/CCL20 in human B cells. *Blood* 2000;**96**:2338−45.
28. Moës B, Li H, Molina Ortiz P, Radermecker C, Rosu A, Vande Catsyne CA, et al. INPP5K controls the dynamic structure and signaling of wild-type and mutated, leukemia-associated IL-7 receptors. *Blood* 2023;**141**:1708−17.
29. Peng SL. The T-box transcription factor T-bet in immunity and autoimmunity. *Cell Mol Immunol* 2006;**3**:87−95.

30. Rudd KE, Johnson SC, Agesa KM, Shackelford KA, Tsoi D, Kievlan DR, et al. Global, regional, and national sepsis incidence and mortality, 1990-2017: analysis for the Global Burden of Disease Study. *Lancet* 2020;**395**:200−11.
31. Shalova Irina N, Lim Jyue Y, Chittezhath M, Zinkernagel Annelies S, Beasley F, Hernández Jiménez E, et al. Human monocytes undergo functional re-programming during sepsis mediated by hypoxia-inducible factor-1Aα. *Immunity* 2015;**42**:484−98.
32. Venet F, Monneret G. Advances in the understanding and treatment of sepsis-induced immunosuppression. *Nat Rev Nephrol* 2017;**14**:121−37.
33. Evans L, Rhodes A, Alhazzani W, Antonelli M, Coopersmith CM, French C, et al. Surviving sepsis campaign: international guidelines for management of sepsis and septic shock 2021. *Intensive Care Med* 2021;**47**:1181−247.
34. Liu D, Huang SY, Sun JH, Zhang HC, Cai QL, Gao C, et al. Sepsis-induced immunosuppression: mechanisms, diagnosis and current treatment options. *Mil Med Res* 2022;**9**:56.
35. Network VNARFT, Palevsky PM, Zhang JH, O'Connor TZ, Chertow GM, Crowley ST, et al. Intensity of renal support in critically ill patients with acute kidney injury. *N Engl J Med* 2008;**359**:7−20.
36. Wang LY, Cui JJ, Ouyang QY, Zhan Y, Wang YM, Xu XY, et al. Complex analysis of the personalized pharmacotherapy in the management of COVID-19 patients and suggestions for applications of predictive, preventive, and personalized medicine attitude. *EPMA J* 2021;**12**:307−24.
37. Leventogiannis K, Kyriazopoulou E, Antonakos N, Kotsaki A, Tsangaris I, Markopoulou D, et al. Toward personalized immunotherapy in sepsis: the PROVIDE randomized clinical trial. *Cell Rep Med* 2022;**3**:100817.
38. Sun J, Zhang X, Ma L, Yang Y, Li X. Clinical study of rhGM-CSF for the treatment of pulmonary exogenous acute respiratory distress syndrome by modulating alveolar macrophage subtypes: a randomized controlled trial. *Medicine (Baltim)* 2023;**102**:e33770.
39. Miyoshi S, Hamada H, Ito R, Katayama H, Irifune K, Suwaki T, et al. Usefulness of a selective neutrophil elastase inhibitor, sivelestat, in acute lung injury patients with sepsis. *Drug Des Devel Ther* 2013;**7**:305−16.
40. Triantafyllou E, Gudd CLC, Mawhin MA, Husbyn HC, Trovato FM, Siggins MK, et al. PD-1 blockade improves Kupffer cell bacterial clearance in acute liver injury. *J Clin Investig* 2021;**131**:e140196.
41. Li H, Limenitakis JP, Greiff V, Yilmaz B, Schären O, Urbaniak C, et al. Mucosal or systemic microbiota exposures shape the B cell repertoire. *Nature* 2020;**584**:274−8.
42. Liu K, Cui JJ, Zhan Y, Ouyang QY, Lu QS, Yang DH, et al. Reprogramming the tumor microenvironment by genome editing for precision cancer therapy. *Mol Cancer* 2022;**21**:98.
43. Cancro MP, Tomayko MM. Memory B cells and plasma cells: the differentiative continuum of humoral immunity. *Immunol Rev* 2021;**303**:72−82.
44. Lenti MV, Luu S, Carsetti R, Osier F, Ogwang R, Nnodu OE, et al. Asplenia and spleen hypofunction. *Nat Rev Dis Primers* 2022;**8**:71.
45. Ihlow J, Michaelis E, Greuel S, Heynol V, Lehmann A, Radbruch H, et al. B cell depletion and signs of sepsis-acquired immunodeficiency in bone marrow and spleen of COVID-19 deceased. *Int J Infect Dis* 2021;**103**:628−35.
46. Kaneko N, Kuo HH, Boucau J, Farmer JR, Allard-Chamard H, Mahajan VS, et al. Loss of Bcl-6-expressing T follicular helper cells and germinal centers in COVID-19. *Cell* 2020;**183**:143-57.e13.
47. Torres LK, Pickkers P, van der Poll T. Sepsis-induced immunosuppression. *Annu Rev Physiol* 2022;**84**:157−81.
48. Liu K, Ouyang QY, Zhan Y, Yin H, Liu BX, Tan LM, et al. Pharmacoepitranscriptomic landscape revealing m^6A modification could be a drug-effect biomarker for cancer treatment. *Mol Ther Nucleic Acids* 2022;**28**:464−76.
49. Tao L, Zhou Y, Luo Y, Qiu J, Xiao Y, Zou J, et al. Epigenetic regulation in cancer therapy: from mechanisms to clinical advances. *MedComm* 2024;**3**:e59.
50. Du J, Liao W, Liu W, Deb DK, He L, Hsu PJ, et al. N^6-adenosine methylation of socs1 mRNA is required to sustain the negative feedback control of macrophage activation. *Dev Cell* 2020;**55**:737-53.e7.
51. Liu Y, Song R, Zhao L, Lu Z, Li Y, Zhan X, et al. m^6A demethylase ALKBH5 is required for antibacterial innate defense by intrinsic motivation of neutrophil migration. *Signal Transduct Target Ther* 2022;**7**:194.
52. Zhang S, Guan X, Liu W, Zhu Z, Jin H, Zhu Y, et al. YTHDF1 alleviates sepsis by upregulating WWP1 to induce NLRP3 ubiquitination and inhibit caspase-1-dependent pyroptosis. *Cell Death Discov* 2022;**8**:244.
53. Wang X, Ding Y, Li R, Zhang R, Ge X, Gao R, et al. N^6-methyladenosine of Spi2a attenuates inflammation and sepsis-associated myocardial dysfunction in mice. *Nat Commun* 2023;**14**:1185.
54. Zhang H, Liu J, Zhou Y, Qu M, Wang Y, Guo K, et al. Neutrophil extracellular traps mediate m^6A modification and regulates sepsis-associated acute lung injury by activating ferroptosis in alveolar epithelial cells. *Int J Biol Sci* 2022;**18**:3337−57.
55. Jackson RJ, Hellen CU, Pestova TV. The mechanism of eukaryotic translation initiation and principles of its regulation. *Nat Rev Mol Cell Biol* 2010;**11**:113−27.
56. Chen B, Chen Y, Rai KR, Wang X, Liu S, Li Y, et al. Deficiency of eIF4B increases mouse mortality and impairs antiviral immunity. *Front Immunol* 2021;**12**:723885.
57. Anderson R, Agarwal A, Ghosh A, Guan BJ, Casteel J, Dvorina N, et al. *eIF2A*-knockout mice reveal decreased life span and metabolic syndrome. *FASEB J* 2021;**35**:e21990.